OULU 2018
C 642

ACTA UNIVERSITATIS OULUENSIS

Ilari Vallivaara

SIMULTANEOUS LOCALIZATION AND MAPPING USING THE INDOOR MAGNETIC FIELD

UNIVERSITY OF OULU GRADUATE SCHOOL;
UNIVERSITY OF OULU,
FACULTY OF INFORMATION TECHNOLOGY AND ELECTRICAL ENGINEERING

ACTA UNIVERSITATIS OULUENSIS
C Technica 642

ILARI VALLIVAARA

SIMULTANEOUS LOCALIZATION AND MAPPING USING THE INDOOR MAGNETIC FIELD

Academic dissertation to be presented with the assent of the Doctoral Training Committee of Technology and Natural Sciences of the University of Oulu for public defence in Auditorium TS101, Linnanmaa, on 12 January 2018, at 12 noon

UNIVERSITY OF OULU, OULU 2018

Copyright © 2018
Acta Univ. Oul. C 642, 2018

Supervised by
Professor Juha Röning

Reviewed by
Professor Hyun Myung
Professor Michael Mascagni

Opponent
Professor Thomas Schön

ISBN 978-952-62-1773-4 (Paperback)
ISBN 978-952-62-1774-1 (PDF)

ISSN 0355-3213 (Printed)
ISSN 1796-2226 (Online)

Cover Design
Raimo Ahonen

JUVENES PRINT
TAMPERE 2018

Vallivaara, Ilari, Simultaneous localization and mapping using the indoor magnetic field.
University of Oulu Graduate School; University of Oulu, Faculty of Information Technology and Electrical Engineering
Acta Univ. Oul. C 642, 2018
University of Oulu, P.O. Box 8000, FI-90014 University of Oulu, Finland

Abstract

The Earth's magnetic field (MF) has been used for navigation for centuries. Man-made metallic structures, such as steel reinforcements in buildings, cause local distortions to the Earth's magnetic field. Up until the recent decade, these distortions have been mostly considered as a source of error in indoor localization, as they interfere with the compass direction. However, as the distortions are temporally stable and spatially distinctive, they provide a unique magnetic landscape that can be used for constructing a map for indoor localization purposes, as noted by recent research in the field.

Most approaches rely on manually collecting the magnetic field map, a process that can be both tedious and error-prone. In this thesis, the map is collected by a robotic platform with minimal sensor equipment. It is shown that a mere magnetometer along with odometric information suffices to construct the map via a simultaneous localization and mapping (SLAM) procedure that builds on the Rao-Blackwellized particle filter as means for recursive Bayesian estimation. Furthermore, the maps are shown to achieve decimeter level localization accuracy that combined with the extremely low-cost hardware requirements makes the presented methods very lucrative for domestic robots. In addition, general auxiliary methods for effective sampling and dealing with uncertainties are presented.

Although the methods presented here are devised in mobile robotics context, most of them are also applicable to mobile device-based localization, for example, with little modifications. Magnetic field localization offers a promising alternative to WiFi-based methods for achieving GPS-level localization indoors. This is motivated by the rapidly growing indoor location market.

Keywords: localization, magnetic field, mapping, mobile robotics, particle filter, SLAM

Vallivaara, Ilari, Samanaikainen paikannus ja kartoitus sisätilojen magneettikentän avulla.
Oulun yliopiston tutkijakoulu; Oulun yliopisto, Tieto- ja sähkötekniikan tiedekunta
Acta Univ. Oul. C 642, 2018
Oulun yliopisto, PL 8000, 90014 Oulun yliopisto

Tiivistelmä

Maan magneettikenttään perustuvat kompassit ovat ohjanneet merenkäyntiä vuosisatojen ajan. Rakennusten metallirakenteet aiheuttavat paikallisia häiriöitä tähän magneettikenttään, minkä vuoksi kompasseja on pidetty epäluotettavina sisätiloissa. Vasta viimeisen vuosikymmenen aikana on huomattu, että koska nämä häiriöt ovat ajallisesti pysyviä ja paikallisesti hyvin erottelevia, niistä voidaan muodostaa jokaiselle rakennukselle yksilöllinen häiriöihin perustuva magneettinen kartta, jota voidaan käyttää sisätiloissa paikantamiseen.

Suurin osa tämänhetkisistä magneettikarttojen sovelluksista perustuu kartan käsin keräämiseen, mikä on sekä työlästä että tarjoaa mahdollisuuden inhimillisiin virheisiin. Tämä väitöstutkimus tarttuu ongelmaan laittamalla robotin hoitamaan kartoitustyön ja näyttää, että robotti pystyy itsenäisesti keräämään magneettisen kartan hyödyntäen pelkästään magnetometriä ja renkaiden antamia matkalukemia. Ratkaisu perustuu faktoroituun partikkelisuodattimeen (RBPF), joka approksimoi täsmällistä rekursiivista bayesilaista ratkaisua. Robotin keräämien karttojen tarkkuus mahdollistaa paikannuksen n. 10 senttimetrin tarkkuudella. Vähäisten sensori- ja muiden vaatimusten takia menetelmä soveltuu erityisen hyvin koti- ja parvirobotiikkaan, joissa hinta on usein ratkaiseva tekijä.

Tutkimuksessa esitellään lisäksi uusia apumenetelmiä tehokkaaseen näytteistykseen ja epävarmuuden hallintaan. Näiden käyttöala ei rajoitu pelkästään magneettipaikannukseen- ja kartoitukseen.

Robotiikan sovellusten lisäksi tutkimusta motivoi voimakkaasti kasvava tarve älylaitteissa toimivalle sisätilapaikannukselle. Tämä avaa uusia mahdollisuuksia paikannukselle ympäristöissä, joissa GPS ei perinteisesti toimi.

Asiasanat: kartoitus, magneettikenttä, mobiilirobotiikka, paikannus, partikkelisuodatin, SLAM

I always ask myself:
"How can I be more like a spiny lobster today?"
Now I’ll be one step closer to my goal

ANONYMOUS COWARD
Comment on news.slashdot.org about magnetic
field-based localization and IndoorAtlas

Preface

I still remember vividly sitting in the 3rd floor CSE lobby at the University of Oulu almost ten years ago and waiting for my turn for a job interview. I had applied as a mathematics major for a research assistant's position in embedded systems without any experience in the field. The interviewers were stern-faced Anssi and comparably kind-looking Janne, and somehow I managed to convince them to give me the position. Due to my background the job description was changed from embedded systems to more theoretical robotics research, and that is how I joined the CSE Robotics Group.

At first I worked on evolutionary and swarm robotics and Ant Colony Optimization. However, after a while my advisor Dr. Janne Haverinen started talking more and more about Spiny Lobsters and their magnificent ability to navigate in the magnetic field. He was convinced that mobile robots should be able to do the same. After he got promising seminal results in localization [1], I was encouraged to try simultaneous localization and mapping based on the collected magnetic field data. The first prototype used a swarm robotics simulator [2] and a graphics-library to smooth the magnetic field maps represented as RGB images. The results were promising, and my PhD topic clarified soon after. It has been very interesting to see a methodology rise in so little time: when I started my research, there were only a few research papers describing the use of magnetic field maps for localization, and most of those did it only to correct the compass-provided heading. Tackling such a new field has been both frustrating and rewarding.

As smartphones became more common, the concept of indoor magnetic field localization was refined into a business idea. I was honored being asked to be one of the co-founders of IndoorAtlas Ltd. It is a rare and fortunate situation to be able to transfer your academic knowledge and interests so directly to commercial use.

It has been a long and rewarding journey from sitting nervously in the CSE Lobby to be working full-time in a growing start-up company. I am most grateful for the opportunities I have been given. Research-wise, if I were to do the experiments and write the papers now, I would most certainly do many things differently. But I guess that is an essential part of the of this journey after all.

Acknowledgements

First I want to thank my supervisor Prof. Juha Röning for the support he gave me during this journey, the funding he fought for me, and, most importantly, the trust and freedom he gave me in my research. His comments and suggestions on the publications were highly valuable. I also want to express my gratitude to my advisor Dr. Janne Haverinen, who introduced me into probabilistic robotics and magnetic field localization. I would not be here without his open-mindedness about new ideas, encouragement, and enthusiasm about Spiny Lobsters. In general, working at CSE has been a joy. A significant part of this were the colleagues, especially my co-authors Anssi Kemppainen and Katja Poikselkä.

The reviewers of my thesis, Prof. Hyun Myung and Prof. Michael Mascagni, deserve my deepest gratitude. They gave their time and effort to review the manuscript and offered me highly valuable comments to improve my thesis.

Of course, friends and family are important as well. I want to thank all my friends for being my friends. Additionally, I want to thank some of my friends for the wonderful research-related discussions and advice, so thank you Jukka, Kalle, and Valtteri. I'm grateful to my grandparents for moving to Oulu for their kids to get a university degree (skipped the generation, though) and the positive attitude towards education that has been surrounding me my whole life. This was further reinforced by my childhood family and the excellent teachers I've had along the way. Thank you Taina and Enska and all extended and other siblings and family for your encouragement and support.

Staying alive while pursuing your dreams is also important. Therefore I want to thank Infotech Oulu and Academy of Finland for making this financially possible. Later on, the research was tied to reality when working at IndoorAtlas. I want to thank all my co-workers there for making it possible.

Finally, I want to thank Ella. You've been there.

In Oulu, November 2017
Ilari Vallivaara

List of symbols and abbreviations

Mathematical notations

$(d_{i,j})$	*distance matrix, where elements* $d_{i,j} = d(i,j)$ *are pairwise distances between states* i *and* j *(defined by distance function* d*)*
$\|\|\mathbf{x}\|\|$	*Euclidean norm of vector* $\boldsymbol{x}$
$\mathbf{x}_{x,y}$	*vector consisting of* x *and* y *components of vector* $\boldsymbol{x}$
$\|x\|$	*absolute value of number* x
$\|X\|$	*number of elements in set* X
$(x,y,z)^T$	*vector with scalar elements* x,y,z
$x \propto y$	x *is proportional to* y
$X \sim f$	*random variable* X *has distribution* f

Abbreviations

2D, 3D	*two-dimensional, three-dimensional*
API	*application programming interface*
BLE	*Bluetooth Low Energy*
BT	*Bayes' theorem*
cdf	*cumulative density function*
CPU	*central processing unit*
DTW	*dynamic time warping*
GP	*Gaussian Process*
GPS	*global positioning system*
i.i.d.	*independent and identically distributed*
IMU	*inertial measurement unit*
kNN	*k nearest neighbors*
LTP	*Law of total probability*
MA	*Markov assumption*
MC	*Monte Carlo*
MCL	*Monte Carlo localization*
MF	*magnetic field*
MSE	*mean square error*

pdf	*probability density function*
pmf	*probability mass function*
PF	*particle filter*
PDR	*pedestrian dead reckoning*
RBPF	*Rao-Blackwellized particle filter*
RMSE	*root mean square error*
SIR	*sampling importance resampling*
SIS	*sequential importance sampling*
std	*standard deviation*
SLAM	*simultaneous localization and mapping*
T, μT	*tesla, microtesla*
w.r.t.	*with respect to*
QMC	*Quasi-Monte Carlo*

Symbols

$\mathbb{1}_A(\mathbf{x})$	*indicator function:* $\mathbb{1}_A(\boldsymbol{x}) = 1$*, when* $\boldsymbol{x} \in A$*, and* 0 *otherwise*
η	*normalization constant (depending on context)*
$\delta_{\mathbf{x}}(\mathbf{x}_0)$	*Dirac delta function:* $\delta_{\boldsymbol{x}}(\boldsymbol{x}_0) = \delta(\boldsymbol{x} - \boldsymbol{x}_0)$
$\delta_{\mathbf{x}}(A)$	*Dirac measure:* $\delta_{\boldsymbol{x}}(A) = \mathbb{1}_A(\boldsymbol{x})$
θ	*yaw or heading of a robot or magnetic measurement vector on a plane*
$\mathbf{B}$	*magnetic field vector consisting of three scalar components:* $\boldsymbol{B} = (B_x, B_y, B_z)^T \in \mathbb{R}^3$ *(in this thesis in* μT*).*
$E_f[\mathbb{X}]$	*expected value of random variable* $\mathbb{X}$
$m^{(k)}$	*map corresponding to particle k*
$m(\mathbf{x})$	*map function that maps states to MF vectors;* $m(\boldsymbol{x}) : X \to \mathbb{R}^3$
$N(\mu, \sigma^2)$	*normal distribution with mean* μ *and variance* σ^2
$p(A)$	*probability of event A,* $p(A) = p(\boldsymbol{x} \in A) = \int_A p(\boldsymbol{x}) d\boldsymbol{x}$
$p(A\|B)$	*conditional probability of A given B*
$p(\cdot)$	*probability density function*
$p(\mathbf{x})$	*abbreviation for probability* $p(\mathbb{X} = \boldsymbol{x})$
$p(\mathbf{x}_t\|Z_t, U_t)$	*posterior density; belief at time t*
$bel(\mathbf{x}_t)$	*belief function over states at time t,* $bel(\boldsymbol{x}_t) = p(\boldsymbol{x}_t\|Z_t, U_t)$
$\overline{bel}(\mathbf{x}_t)$	*belief function before incorporating the latest measurement,* $p(\boldsymbol{x}_t\|Z_{t-1}, U_t)$
X	*set of states, state space; for poses* $X \subseteq \{(\boldsymbol{x}_{x,y}, \theta) \in \mathbb{R}^2 \times \mathbb{S}\}$

$\mathbb{S}$	*rotation space:* $\mathbb{S} = [0, 2\pi[$
$\mathbf{x}$	*state belonging to the state space,* $\boldsymbol{x} = (x, y, \theta) \in \mathbb{R}^2 \times \mathbb{S}$*, where* $\boldsymbol{x}_{x,y}$ *is the spatial coordinate and* θ *is the heading*
t	*time step corresponding to a discrete moment in time*
$\mathbf{u}_t$	*control for the robot at time t*
U_t	*ordered set of controls* $U_{1:t} = \{\boldsymbol{u}_1, ..., \boldsymbol{u}_t\}$
P	*number of particles* $P = \lvert\{\boldsymbol{x}_t^{(i)}\}\rvert$
$\mathbb{R}^n$	*Euclidean n-dimensional space*
x, y, z	*Cartesian* x, y*, and* z *coordinates*
$\mathbf{x}_t$	*state at time t*
$w_t^{(i)}$	*importance factor (weight) of particle* $\boldsymbol{x}_t^{(i)}$ *at time t*
$\hat{\mathbf{x}}$	*estimate or approximation of* $\boldsymbol{x}$
σ	*standard deviation*
$\mathcal{X}_t$	*set of particles* $\{\boldsymbol{x}_t^{(i)}\}$ *at time t, where* $\boldsymbol{x}_t^{(i)} \in X$
$\mathbf{x}_t^{(i)}$	*particle i at time t*
X_t	*trajectory consisting of ordered poses* $X_{1:t} = \{\boldsymbol{x}_1, ..., \boldsymbol{x}_t\}$
$\mathbf{z}$	*measurement or magnetic field measurement,* $\boldsymbol{z} = (z_x, z_y, z_z)^T \in \mathbb{R}^3$*, where* z_x, z_y, z_z *are the three components of the magnetic field*
$\mathbf{z}^{\perp}$	*yaw-independent measurement,* $\boldsymbol{z}^{\perp} = (\lvert\lvert z_{x,y} \rvert\rvert, z_z)^T$
Z_t	*ordered set of collected measurements* $Z_{1:t} = \{\boldsymbol{z}_1, ..., \boldsymbol{z}_t\}$

List of original publications

This thesis is based on the following articles, which are referred to in the text by their Roman numerals:

I Vallivaara I, Haverinen J, Kemppainen A & Röning J (2010) Simultaneous localization and mapping using ambient magnetic field. In: Multisensor Fusion and Integration for Intelligent Systems (MFI), 2010 IEEE Conference on, pp. 14–19

II Vallivaara I, Haverinen J, Kemppainen A & Röning J (2011) Magnetic field-based SLAM method for solving the localization problem in mobile robot floor-cleaning task. In: Advanced Robotics (ICAR), 2011 15th International Conference on, pp. 198–203

III Vallivaara I, Kemppainen A, Poikselkä K & Röning J (2013) Monty Hall particle filter: A new method to tackle predictive model uncertainties. In: Advanced Robotics (ICAR), 2013 16th International Conference on, pp. 1–8

IV Vallivaara I, Poikselkä K, Rikula P & Röning J (2016) Systematic alias sampling: An efficient and low-variance way to sample from a discrete distribution. ACM Transactions on Mathematical Software (TOMS) 43(3): 18

V Vallivaara I, Poikselkä K, Kemppainen A & Röning J (2017) Quadtree-based ancestry tree maps for 2D scattered data SLAM. Manuscript

Contents

Abstract

Tiivistelmä

Preface **9**

Acknowledgements **11**

List of symbols and abbreviations **13**

List of original publications **17**

Contents **19**

1 Introduction **23**

1.1 Background 23

1.2 Motivation 24

1.2.1 Human use of indoor MF maps 25

1.2.2 Magnetometer as the lone sensor 26

1.2.3 SLAM with similar sensors 26

1.3 Problem and hypothesis 26

1.4 Scope and approach 27

1.5 Contribution and summary of original papers 28

1.5.1 Author's contribution 29

2 Indoor magnetic field **31**

2.1 Introduction 31

2.2 Definitions and assumptions 31

2.3 Earth's magnetic field 34

2.4 Distortions caused by metal structures 34

2.5 Spatial variation: how informative is a single measurement? 35

2.6 Temporal stability and effect of metallic objects 37

2.7 Modeling the magnetic field 40

2.8 Conclusions 41

3 Recursive state estimation **43**

3.1 Introduction 43

3.2 Discrete-time state space model 44

3.3 Bayes filter 44

3.4 Particle filter 47
3.4.1 Standard particle filter algorithm 47
3.4.2 Importance factor 48
3.4.3 Motion model 51
3.4.4 Measurement model 51
3.4.5 Resampling 52
3.4.6 Estimates and density extraction 53
3.5 Sampling variance 53
3.5.1 Improving the proposal approximation 54
3.6 Example: Monte Carlo localization on the magnetic landscape 56
3.6.1 Controls and Motion model 57
3.6.2 Measurements, Measurement model, and Resampling 57
3.6.3 Localization along a simulated trajectory 57
3.6.4 Note on multimodality - signal as a random walk 60
3.7 Conclusions 60
4 Magnetic field navigation and localization 61
4.1 Introduction 61
4.2 Magnetoreception in animals 62
4.3 Early work 62
4.4 Localization methods 63
4.5 Magnetic field map model 64
4.6 Mobile devices 64
4.7 Conclusions 65
5 Simultaneous localization and mapping 67
5.1 Introduction 67
5.2 Rao-blackwellized particle filter 68
5.3 Map representation 68
5.3.1 Bottleneck: memory and resampling 69
5.4 Loop closing 70
5.4.1 Example on MF-based loop closing 72
5.5 SLAM in the magnetic field 74
5.5.1 VF-SLAM and its MF derivations 74
5.5.2 Bathymetric SLAM 76
5.5.3 FootSLAM and MagSLAM 77
5.5.4 Graph-based approaches 77

5.6 Conclusions . . . 78
6 Conclusions and future directions **81**
References **83**
Original articles **93**

1 Introduction

1.1 Background

The ability to localize itself is one of the most vital abilities for an autonomous mobile agent. The localization problem is considered one of the most fundamental ones in mobile robotics [8, 9]. Whether you are a mobile robot or human, in order to make informed decisions and planning, you have to be able to differentiate where you are. Humans are usually able to make this automatically via visual and other clues, but in robotics, robust localization is an active research topic. Robotics localization is a vast research field, influencing many application domains from self-driving cars to simple domestic robots, such as autonomous vacuum cleaners [10–12].

Simultaneous localization and mapping (SLAM) takes the problem one step further and requires the robot to collect the map while localizing itself. Traditionally, SLAM in robotics has been tackled with laser or vision-based approaches. The most common map representations are *feature-based*, where the map consists of discriminative features in the environment, such as tree trunks, or *occupancy grid-based*, where the map is represented by a dense grid where each cell represents its probability of being occupied. However, recently, also more unconventional sensor modalities for SLAM have gained attention. Often, these sensors are of lower quality due to their very low-cost or ability to measure only one point in space at a time. This makes SLAM by using such sensors, e.g., magnetometers [3, 13], depth sensors [14], or WiFi receivers [15], more challenging but still possible. However, the lower price point makes them applicable in many application domains where, e.g., a laser range finder would not be suitable. For example, many modern smart phones include a sensor setup consisting of magnetometer, barometer, WiFi receiver, light sensor, often accompanied with accelerometer and gyroscope. The sensors make movement tracking possible via inertial measurement unit (IMU). Cadena et al. [9] provide a very current (2016) view on the state of SLAM, including open problems, and also briefly discuss novel sensor modalities.

Distortions in the Earth's magnetic field have been usually seen as a source of error for compasses and magnetometers. However, in their work Haverinen et al. [16] showed that the anomalies in indoor magnetic field can be manually collected to build a map that can be utilized to localize both robots and humans equipped with wearable sensors. Figure 1 illustrates how modern indoor environment at the University of Oulu

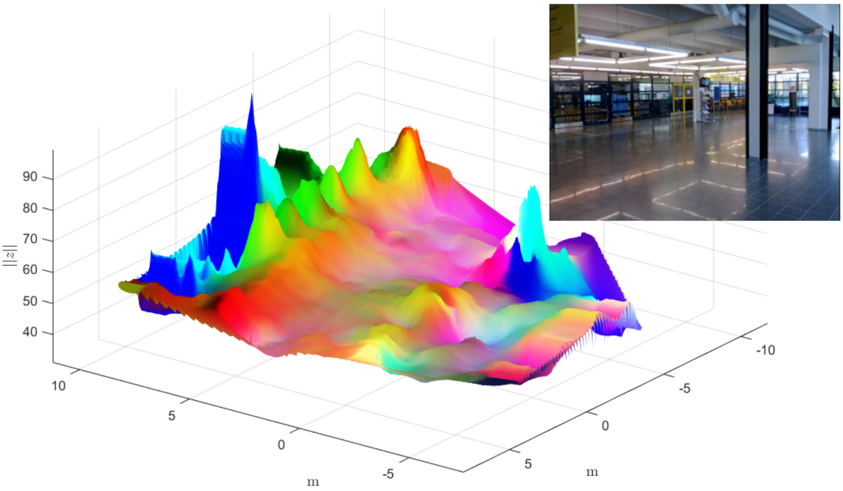

Fig. 1. The magnetic landscape in Discus Entrance Hall at the University of Oulu. The figure illustrates the strong variation in a modern office environment. Magnitude (μT) of the magnetic field is depicted as the height of the surface, and the color illustrates the direction of the vector. The significant anomalies caused by steel in the pillars can be clearly seen in the landscape.

has strong variation in the magnetic fields and the resulting magnetic landscape. The arduous magnetic data collection can be partly automatized by using a mobile robot that solves the SLAM problem relying solely on the magnetic field data (Publication I). Furthermore, the acquired maps are accurate enough to be used in mobile robot cleaning task, with an accuracy of approximately 10 cm in a modern office building environment (Publication II).

1.2 Motivation

The motivation for magnetic field-based SLAM (MF-SLAM) research is three-fold. The first motivation is to automatically provide MF maps for other agents, e.g. for human users. This could include equipping the robot with other, possibly high-quality, sensors for higher precision with or without sensor fusion. The second motivation is using the MF as the only external signal (coupled possibly with odometry), yielding a system with very minimal sensor requirements. The final motivation is providing SLAM methods for sensor data that is similar to the magnetic field measurements. These three main aspects are discussed shortly in the next subsections.

1.2.1 Human use of indoor MF maps

For outdoor localization, GPS has established itself as the dominant technology for common everyday use, running on billions of consumer-grade devices. It is used to power huge domains from navigation to very recently surfaced augmented reality applications, such as the highly popular Pokémon Go that added 7.5 billion dollars to Nintendo's stock value almost overnight [17]. For indoor localization, this is not the case, and there is not a single established method for localization. Indoors, where GPS does not work, there is an ongoing battle of technologies to claim the throne of "indoor-GPS".

Indoor positioning systems are becoming more and more viable in consumer grade devices, such as smart phones and tablets. With estimated 4.4 billion dollar indoor location market in 2019 [18], indoor localization with mobile devices has become an active research topic. Lymberopoulos et al. [19] evaluate 22 different indoor localization technologies attending 2014 Microsoft Indoor Localization Competition. The reported localization errors range from 0.72 m to 10.22 m. Despite three top competitors [20–22] achieving localization error less than 2 m, the authors conclude that the indoor localization problem is not solved to offer GPS-like performance due to inconsistencies in accuracy, sensibility to environment changes, and high costs of deployment for both infrastructure-based and infrastructure-free solutions.

Despite its shortcomings [23, 24], using WiFi signal maps is the most common method for indoor localization. Magnetic field-based localization is one of the promising technologies for indoor localization, as the indoor magnetic field is temporally stable, requires no hardware installation, and often yields comparable or better results to WiFi-based localization [24–26]. However, the cost of collecting a comprehensive MF map can be high [25, 27, 28], as it is most often performed manually, sometimes with a dedicated application [24, 25, 29]. Figure 2 (a) illustrates the mapping process using IndoorAtlas MapCreator 2 application [29]. Reducing these map collection costs with automated SLAM systems like the ones presented in this thesis or in [28] could make large scale collecting of dense maps significantly more plausible.

1.2.2 Magnetometer as the lone sensor

The main problem addressed in this thesis is SLAM using only magnetometer readings and odometry. A clear advantage of the minimal sensor requirements of the presented methods is that they are applicable on very low-end and low-cost robotic platforms, such as often used in swarm robotics, thus making the solution possibly very scalable. If the achieved accuracy permits for example room-to-room navigation in apartment-sized environments, it is often perfectly sufficient for domestic robotics. Another advantage of the minimal setup is that it sets a lower bound for SLAM performance that can be easily improved by adding other sensors.

1.2.3 SLAM with similar sensors

Many sensor measurements, such as depth, WiFi, and light intensity, are similar to magnetometer readings. They provide scattered data from which a signal map can be constructed. Because of their similarity, also the applicable methods are similar. Figure 2 (b) illustrates a mapped lake environment with three scalar measurements: depth, vegetation, and seafloor density. Although the lake environment in Figure 2 (b) was collected with GPS and manually set route, GPS is not always available, e.g., for autonomous underwater vehicles (AUVs) [14]. The three measurements form a three-component vector that could be utilized in SLAM with the methods presented in this thesis. Furthermore, if the environment contains MF variation, other similar low-cost sensors could be fused in to obtain more informative measurements and maps. This could possibly result in significantly more robust SLAM with almost as minimal sensor requirements as discussed in the previous subsection. This thesis concentrates on MF-SLAM, but the methods presented here should be easily transferable to domains utilizing similar-enough sensors. Addressing these interesting possibilities was left out of the scope of this thesis and are considered topics for future research.

1.3 Problem and hypothesis

The problem consists of a robot operating on bounded but previously unknown 2D planar indoor environment. The robot is equipped with a magnetometer and (wheel) actuators that are able to move it around. The magnetometer provides noisy observations of the indoor magnetic field from one spatial point at a time and the wheel encoders

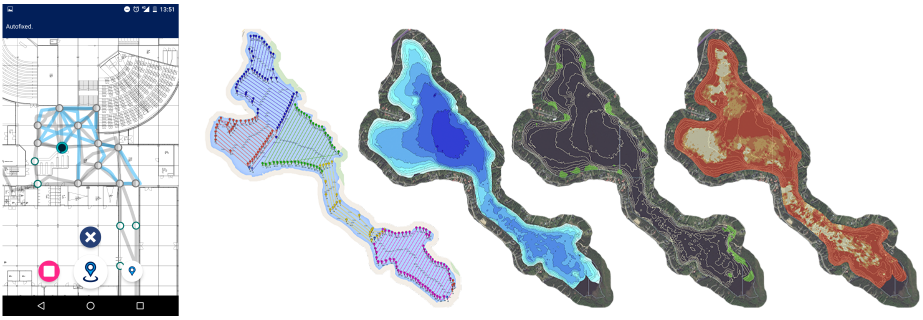

(a) (b)

Fig. 2. (a) Indoor mapping process using publicly available IndoorAtlas MapCreator 2 Android application. Courtesy of IndoorAtlas Ltd [29]. (b) Mapping process of a lake with the resulting depth, vegetation, and seafloor density maps (from left to right). The diameter of the lake is approximately 2.7 km. Courtesy of Aquamarine Robots [30].

provide noisy information about the robot's movement (odometry). The robot is allowed to drive around and it is assumed the odometry is somewhat reliable, i.e., the error in odometry is bounded on short time intervals. This includes that the robot either does not collide with walls (manually driven) or is able to detect collision (bumper sensor). Also it is assumed that the robot is driven so that it crosses its trajectory making map matching and loop closure possible. This is achieved either through control or by physically bounding the environment. The hypothesis is that the indoor magnetic field variations contain enough information that the robot is able to simultaneously collect a map of the magnetic field and localize itself with respect to that map using only the magnetometer and odometry information. The end result is a geometrically correct map of the magnetic landscape in the environment that can be used for localization purposes later on.

1.4 Scope and approach

The problem is approached from the standard probabilistic robotics viewpoint, where the uncertain state of the robot is modeled as a probability distribution over all possible states [8]. To recursively estimate this density, a popular numerical approximation method called the particle filter (PF) is used. The particle filter uses the sensor and odometry data and provides an approximate solution to the underlying recursive Bayesian estimation problem (see Chapter 3).

The research presented in the accompanying Publications I–V is guided by very practical needs and the presented methods and results concentrate on applicability to real-world scenarios. Publications I–II act as feasibility studies to confirm the hypothesis with real-world data. Publications III–V, in their turn, present auxiliary methods that can be used to improve the performance and robustness of the basic idea presented in the first two publications. It should be noted, however, that the presented auxiliary methods are general in nature and not limited to this particular use case. All presented results are empirically validated with as much real-world data as practically reasonable. That said, the contributions of this thesis are not theoretical in nature, but rather propose empirically validated solutions to practical problems.

This overview is structured as follows: Chapter 2 addresses the characteristics of the indoor magnetic field for localization purposes. Chapter 3 shortly presents the theoretical background behind PF-based localization and illustrates the PF solution in MF-localization context. Chapter 4 covers the related work done in the field of MF-localization. Chapter 5 extends the PF approach to handle SLAM and covers literature in MF-SLAM context.

1.5 Contribution and summary of original papers

One of the main contributions of the research presented in the accompanied publications is to validate the feasibility of simultaneous localization and mapping based on indoor magnetic field. Experimental results demonstrate that geometrically consistent 2D maps up to 300 m^2 can be automatically collected from modern buildings utilizing only odometry and a three-axis magnetometer. The large size of the real-life environments used in the experiments is still to be matched with more recent research utilizing similar features [13, 31, 32]. Furthermore, the acquired maps offer localization accuracy measured in decimeter level. With this accuracy and the extremely low sensor requirements, magnetic field localization offers a truly viable alternative to many traditional approaches.

Other main contributions are the proposed novel helper methodology. These include uncertainty handling in sparse magnetic field maps, a general and very efficient sampling method, and a scattered data map representation algorithm that is useful for but not limited to magnetic field SLAM domain. The main contributions of each Publication I–V are presented in the list below.

I The idea of simultaneous localization and mapping is experimentally validated with real world magnetic field data. A randomly driving robot is able to collect geometrically consistent 2D maps of several room-sized environments. The work addresses several practical key aspects of making magnetic field SLAM feasible.

II The mapping process with real world data is further investigated and refined. Magnetic field SLAM is verified in larger lobby-like environments with approximate area of 300 m^2. The paper also evaluates the map quality; the produced maps offer estimated worst case localization accuracy of approximately 10 cm. The accuracy is argued to be sufficient for mobile robot floor-cleaning tasks.

III A method is presented to handle the uncertainty in predictive models that are used to estimate the magnetic field in non-mapped locations. Addressing the problem is crucial with the sparse and uncertain maps inherent in magnetic field SLAM. The proposed method generalizes the conditional weight update rules utilized in Publications I–II and is able to increase robustness of localization without sacrificing much of convergence speed.

IV A general method is described to generate batches of low-variance samples efficiently from a given discrete distribution. The batches can be used for particle propagation when modeling their movement, for example. As the method needs only one random number per patch, it achieves an order-of-magnitude speed improvement over multinomial sampling which is relevant on mobile or embedded devices with low computing power. Furthermore, the decreased variance is demonstrated to improve particle filter performance with low particle counts when the samples are used to propagate the particles.

V The paper describes how the memory and time complexity of the particle filter-based MF-SLAM solution can be improved by using quadtree-based ancestry trees. The presented methodology enables particle counts in tens of thousands and makes some previously unsolvable instances tractable.

1.5.1 Author's contribution

In all of the publications I–V, the author had the main responsibility in writing the article and designing and conducting the experiments. Dr. Haverinen provided expertise on the MF localization and gave advice in publications I–II. Kemppainen wrote the code and text for the Gaussian Process-related parts in I–II and provided technical help in the experiments. Poikselkä and Rikula had a minor but important role in discussing the ideas and details in publications III–V and IV, respectively. Prof. Röning provided useful guidance and feedback on all of the publications I–V.

The author has also participated in writing publications left out of this thesis based on their non-related topic [33, 34] and/or author's minor role [35–39].

2 Indoor magnetic field

2.1 Introduction

Steel structures, such as pillars and rebars (reinforcement bars), are known to cause distortions to the Earth's magnetic field that affect the field significantly, especially in indoor environments [40]. This is illustrated in Figure 3. These distortions are temporally stable and vary spatially, so they offer potentially a way to construct informative magnetic field maps of the environment. This chapter presents a short overview on the literature about the indoor magnetic field studied for its suitability for indoor localization purposes. Magnetic field-based indoor localization itself is addressed in Chapter 4. First, some definitions and assumptions are presented. The magnetic landscape of the University of Oulu Discus Entrance Hall is studied and visualized as an example. Then, the characteristics of the indoor MF, such as variability, temporal stability and effect of moving metallic object, are evaluated based on research addressing these issues for localization purposes [41–44].

2.2 Definitions and assumptions

The definitions and assumptions presented here are inspired by the presentations in Angermann and Frassl et al. [42, 45] and Gutmann et al. [12, 46]. The magnetic field can be thought of a continuous 3D vector field defined spatially everywhere. It can be formalized as a function

$$f_B(\mathbf{x}) : \mathbb{R}^3 \to \mathbb{R}^3 \tag{2.2.1}$$

that maps any Cartesian coordinate $\mathbf{x} = (x, y, z)^T \in \mathbb{R}^3$ to a magnetic field value $\mathbf{B} = (B_x, B_y, B_z)^T$, consisting of three orthogonal components B_i, which are reported in microteslas (μT) in this thesis. The magnetic field can be measured using sensors called magnetometers that report the magnetic field in the sensor coordinate frame. That is, the measurement depends on the sensor's location $\mathbf{x} \in \mathbb{R}^3$ and orientation $\mathbf{r} = (r_x, r_y, r_z)^T \in \mathbb{S}^3$, where r_i denote rotation around the corresponding axis (*pitch, roll, yaw*) and $\mathbb{S} = [0, 2\pi[$. This can be formalized as a *sensing function*

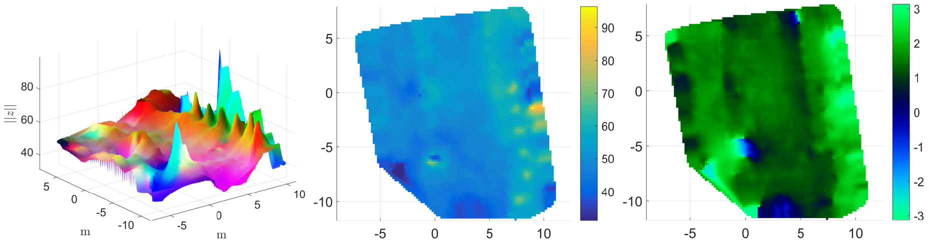

(a) landscape

(b) $||\mathbf{z}||$

(c) direction in horizontal plane

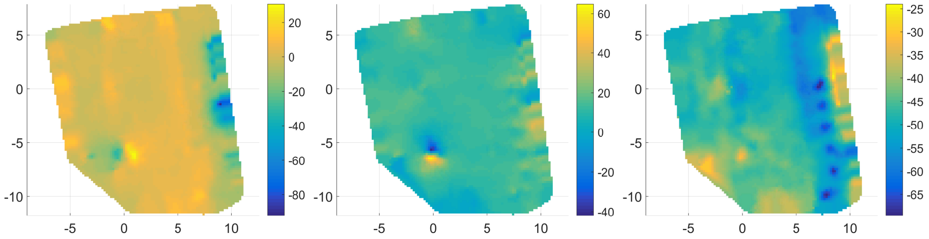

(d) $\mathbf{z}_x$

(e) $\mathbf{z}_y$

(f) $\mathbf{z}_z$

Fig. 3. The magnetic landscape of the Univesity of Oulu Discus entrance hall visualized with respect to different components. The spatial scale is in meters and the MF values in μT.

$$f_s(\mathbf{x}, \mathbf{r}) : \mathbb{R}^3 \times \mathbb{S}^3 \to \mathbb{R}^3 \tag{2.2.2}$$

that maps the magnetic field value to a sensor reading depending on location **x** and rotation **r**. In reality, this function may have many stochastic uncertainties due to such factors as soft and hard iron biases or sensor noise, but for the purposes of this presentation, f_s is assumed to be free of such uncertainties. Magnetometer calibration is discussed in detail, e.g., in [43, 47]. The *map function*

$$m_B(\mathbf{x}) : X \to \mathbb{R}^3 \tag{2.2.3}$$

is an approximation of the MF function f_B, describing it over some subset of Cartesian coordinates $X \subset \mathbb{R}^3$, where X depends on the map representation. The function is also called the *magnetic map* of X, or sometimes *magnetic landscape* of X if the map is dense enough.

Most modern mobile devices include an accelerometer than can sense the gravity vector. This can be used to estimate the sensor's pitch and roll [48], thus leaving the yaw as the remaining rotational degree of freedom. The pitch and roll can be used to extract

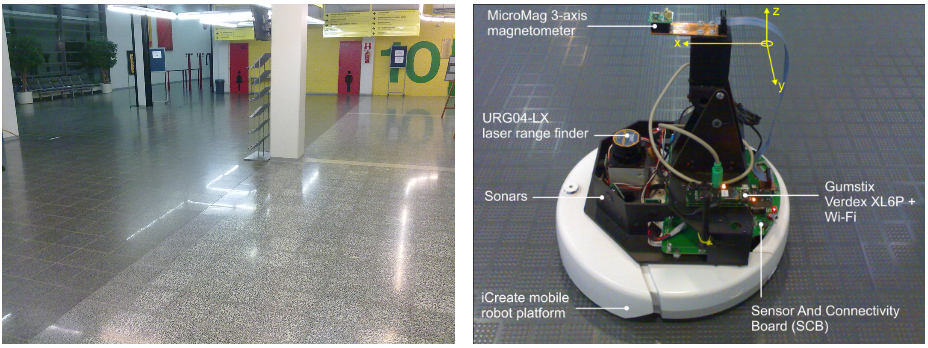
MicroMag 3-axis magnetometer
z
x
y
URG04-LX laser range finder
Sonars
Gumstix Verdex XL6P + Wi-Fi
iCreate mobile robot platform
Sensor And Connectivity Board (SCB)

(a) University of Oulu Discus entrance hall

(b) iRobot Create equipped with a magnetometer

Fig. 4. (a) University of Oulu Discus entrance hall. The dimensions of the main area are about $15m \times 20m = 300m^2$. (b) The robot and the magnetometer used to collect the data. Only the magnetometer is used of the sensors that are part of the sensor connectivity board described in [50].

the vertical component and the horizontal components of the magnetic field by rotating the measurement accordingly [41, 43, 45]. For convenience, notation

$$\mathbf{z}^{\perp} = (||\mathbf{z}_{x,y}||, z_z)^T \tag{2.2.4}$$

for these yaw-independent measurements is adopted. If in addition the z coordinate of the sensor is known, the situation is similar to the case of a mobile robot operating on a 2D plane with a fixed magnetometer. Such a robot is illustrated in Figure 4 (b) and its state can be characterized by its pose $(\mathbf{x}_{x,y}, \theta) \in \mathbb{R}^2 \times \mathbb{S}$, where $\mathbf{x}_{x,y}$ represents the robot's location and θ represents its heading. This simplifies the sensing function to

$$f_s'(\mathbf{x}_{x,y}, \theta) : \mathbb{R}^2 \times \mathbb{S} \to \mathbb{R}^3. \tag{2.2.5}$$

Currently, most MF localization approaches fall into this category [16, 25, 45, 47, 49], but in robotics the situation may tilt towards 3D as drones become more common. For the remainder of the thesis, the z coordinate of the sensor is assumed fixed and the measurements are assumed to be normalized w.r.t. pitch and roll, and the measurement is simply denoted by $\mathbf{z} = (z_x, z_y, z_z)^T \in \mathbb{R}^3$. For the purposes of this thesis we also make the following simplifying but justified assumptions and clarifications:

1. *The magnetic field can be measured.* A sensor (magnetometer) is assumed that is able to measure the MF in the sensor's coordinate frame.

2. *Non-biased sensor.* If the sensor's orientation is known, the measurement can be rotated (normalized) into world coordinates. Subsequently, the measurement can be used to estimate the sensor's orientation at a given location if the MF is known.
3. *The magnetic field varies spatially.* The MF is assumed to be non-constant and to vary in the spatial domain. See, section 2.5.
4. *The magnetic field is temporally stable.* The MF is assumed to be temporally stable, and, e.g., changing electric currents or geomagnetic storms or more long term changes, such as the wandering of the Earth's magnetic poles, are not taken into account. See, section 2.6.
5. *Source and physics agnostic.* Besides noting that the magnetic field is usually non-zero (especially in the horizontal plane), no distinction is made between the main field and the distortions. No attempt is made to infer or model the physical objects that cause the variation in the MF, or to model the magnetic field in a physically correct way, for that matter.

2.3 Earth's magnetic field

The geomagnetic field on the Earth's surface is a combination of fields generated by multiple sources, such as ferromagnetic objects and electrical devices, and it varies from place to place. However, 90% of the field consists of the *main field*, generated by the Earth's outer core, and its magnitude ranges approximately from 25 to 65 μT [51]. The main field changes slowly in time and it can be described with mathematical models, such as the International Geomagnetic Reference Field (IGRF) [52]. The Earth may be approximated as a giant magnetic dipole, and its interaction with other magnetic sources may be modeled as a multiple dipole system, as done in some related work [53]. Because the main field is so dominant in most outdoor scenarios and the compass needle aligns itself with the horizontal component of the Earth's magnetic field – pointing to the magnetic north – the compass has been used for centuries for navigation.

2.4 Distortions caused by metal structures

Because the intensity of a field caused by a steel structure decreases strongly with distance to the magnetic body, the effect of the smaller sources of variation (e.g., rebars) quickly diminishes when not measured in the utmost vicinity, and the lower spatial frequencies start to dominate the field (e.g., steel pillars, elevators). Therefore

Angermann et. al [42] measure the MF as close to the floor as possible to obtain a very detailed landscape. This is done to capture the fine details of the rebar structure under the floor and achieve centimeter level accuracy in localization. Larger structures, such as steel-reinforced pillars and elevator shafts, cause big distortions in the field that can be measured meters away [53–55], e.g., in the middle of a corridor. However, instead of centimeters, the spatial frequency of these variations is typically from few decimeters to meters. Chung et al. [44] report that they can measure distinctive magnetic features within 2.5 cm radius in a middle of a corridor.

Despite acknowledging the physical causes of the anomalies in the MF, no attempt is made in this thesis to model or infer the sources of the magnetic field. The MF is rather seen as an abstract vector field with some desirable properties. A similar approach is taken by Angermann and Frassl et al. [42, 45] in related research where they study the characteristics of the magnetic field for localization and mapping purposes. For explicit physical source modeling in localization context, see the work by Subbu et al. [53, 54], where the effects of pillars and other big objects are modeled based on physical properties of the ferromagnetic material. Similarly, Wahlström et al. [56] derive a Gaussian Process model based on the Maxwell's equations and are able to estimate, e.g., shapes of objects from the MF measurements.

2.5 Spatial variation: how informative is a single measurement?

The Discus entrance hall (Fig. 3 and Fig. 4 (a)) is a typical public indoor space at the University of Oulu main building, with a main area of about 300 m^2. The reinforced pillars and steel structures near the walls cause significant variations in the magnetic landscape, collected about 40 cm height from the floor (Fig. 4 (b)). In order to visualize how distinctive the magnetic measurements actually are, the MF map of the Discus entrance hall is evaluated at poses with fixed heading in different discrete evenly spaced locations. The distance between the MF values at states i and j can be defined in multiple ways (discussed later). The distances can be represented as an $N \times N$ distance matrix $(d_{i,j})$, where each element corresponds to the pairwise distance between the states. The discretization of states is done to make visualization as distance matrices possible. The 288 discrete locations and measurement statistics over the corresponding poses are depicted in Figure 5. Units in the statistics are in μT, except for the heading, the unit is degrees (chosen over radians for visualization). As can be seen, the magnetic field has about 5-10 μT standard deviation depending on the channel.

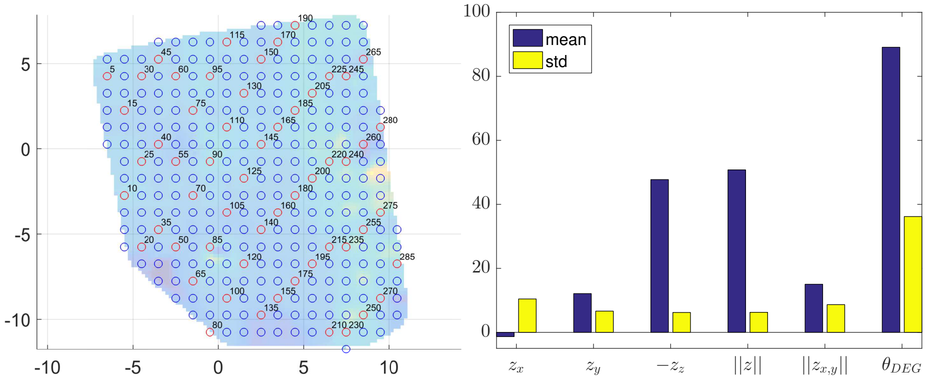

(a) Discrete state space

(b) Means and standard deviations

Fig. 5. (a) Discrete locations ($N = 288$) on Discus entrance hall map. (b) Statistics of different magnetic field features over the locations. The spatial scale is in meters and the MF statistics in μT, except the heading that is in degrees (for similar scale).

If heading is known, the magnetic similarity of two locations can be acquired by comparing the full measurement vectors. However, as the heading is not generally known, the yaw-independent measurement $\mathbf{z}^{\perp} = (||\mathbf{z}_{x,y}||, z_z)^T$ in specific spatial coordinates $\mathbf{x}_{x,y}$ can be expressed as the vertical component $\mathbf{z}_z$ and the norm of the horizontal components $||\mathbf{z}_{x,y}||$ [41, 43, 45]. All possible measurements in $\mathbf{x}_{x,y}$ can be then obtained by rotating $\mathbf{z}_{x,y}$ on the horizontal plane. In illustrations, such as Figure 3, the heading is assumed fixed but arbitrary. Comparing the vector $\mathbf{z}^{\perp}$ describes the situation most accurately when trying to figure out the magnetic similarity of two locations for localization purposes.

In the following the difference between two vectors is computed as the Euclidean distance of their difference, and the distance matrices are computed over the discrete states visualized in Figure 5 (a). The matrix values are clamped between 0 and 20 μT in order to allow easier comparison and more clear visualization. Figures 6 (b-d) illustrate the distance matrices (pairwise distances) of x, y, and z components of the magnetic field. In addition, pairwise spatial distances of the locations are visualized (a) in order to perceive pattern similarities and spatial correlation. Figure 7, in its turn, illustrates the differences associated with the three alternative measurement models presented explicitly in several papers [41, 43, 45]:

(a) *Norm of the measurement.* The least distinctive one is using the difference of the norm of the field, although it has the advantage that the sensor orientation is not required. The distance matrix for $||\mathbf{z}||$ is depicted in Fig. 7(a).

(b) *Norm of the horizontal component and the vertical component.* If direction of gravity can be estimated, $\mathbf{z}^{\perp} = (||\mathbf{z}_{x,y}||, z_z)^T$ can be used to differentiate between locations. This corresponds to the robot localization in planar environments. The distance matrix for $\mathbf{z}^{\perp}$ is depicted in Fig. 7 (b).

(c) *Full measurement vector.* If the sensor orientation is fully known, the locations can be differentiated by the full vector. This is clearly the most distinctive of the three measurement models. The distance matrix for $\mathbf{z}_{x,y,z}$ is depicted in Fig. 7 (c).

For completeness, the yaw-distances are depicted in Figure 7 (d), as heading is used as magnetic signature in some work [49, 57].

2.6 Temporal stability and effect of metallic objects

Obtaining a magnetic field map would be close to useless if it was not temporally stable. The Earth's magnetic field is known to fluctuate on a daily basis due to diurnal cycle, slowly in time due to movement of magnetic poles, and more randomly, e.g., due to geomagnetic storms caused by solar flares. However, for all practical purposes, although measurable, the fluctuations are negligible when compared to the typical variation inside a building. For example, Frassl et al. [45] report that the daily fluctuations in range of 10 nT to 30 nT are less than 0.1% of the average magnitude of $48\mu T$ in their location. Perhaps more importantly, such variations are less than 1% of typical variation inside a modern building (Fig. 5 (b)). For this reason, it is justifiable to ignore the effect of these fluctuations, as done in majority of research [42, 45, 47]. Stability of the magnetic fields is empirically studied further, e.g., in [41, 44, 55, 58]. The overall consensus is that the MF is temporally stable enough for localization purposes.

Another possible cause for changing magnetic field is the moving metallic objects present in modern environments. As the magnetic intensity degrades strongly with distance, several papers have found that small metallic objects, such as watches, phones, and laptops, have very short range of about 15-25 cm in affecting the magnetic field [41, 43, 44, 59]. The effect of massive objects, namely elevator carts, is also studied in the literature. Li et al. [41] report that the activity of two adjacent elevators causes variation in the field intensity up to 7 m away. However, even as close as 1 m, the

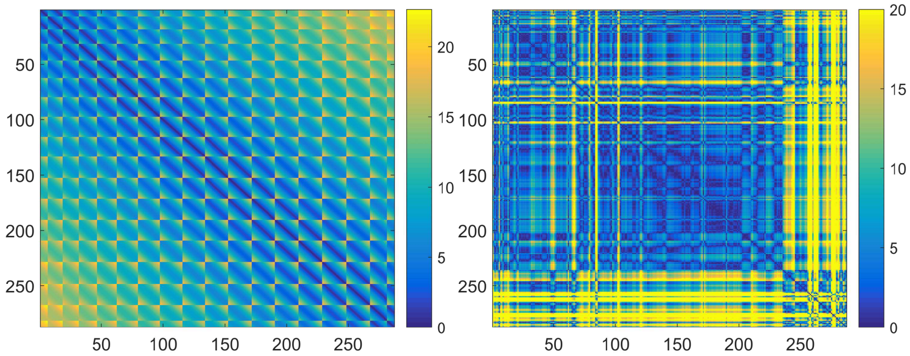

(a) Spatial state distances (b) $\mathbf{z}_x$

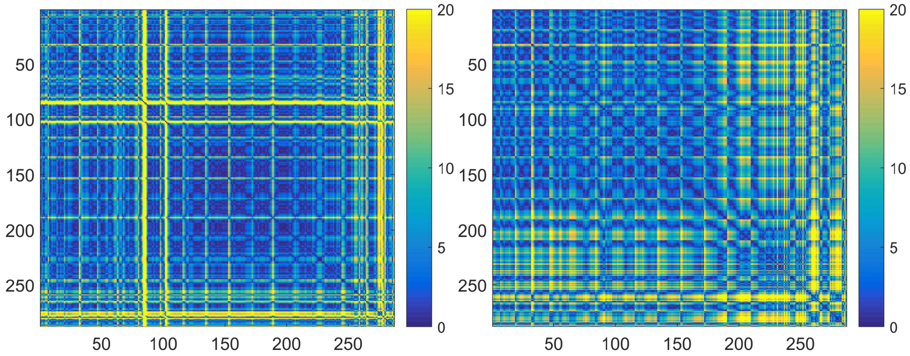

(c) $\mathbf{z}_y$ (d) $\mathbf{z}_z$

Fig. 6. (a) Pairwise spatial state distances and (b-d) channel-wise magnetic field distance matrices for the discrete states depicted in Fig. 5. The spatial distances are in meters and the MF distances in μT.

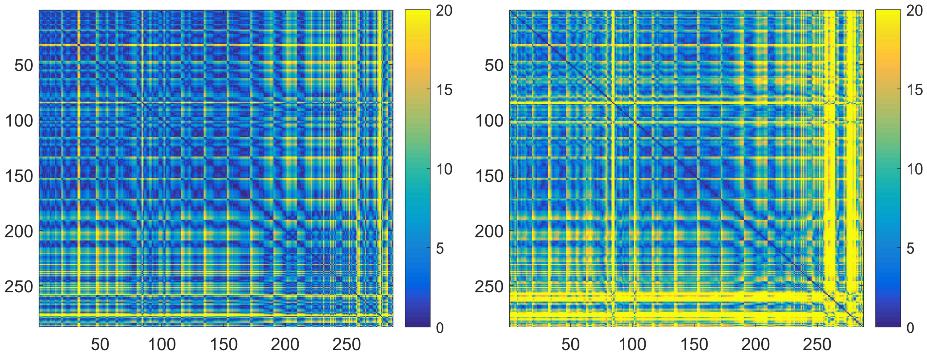

(a) $||\mathbf{z}||$ (b) $(||\mathbf{z}_{x,y}||, z_z)^T$

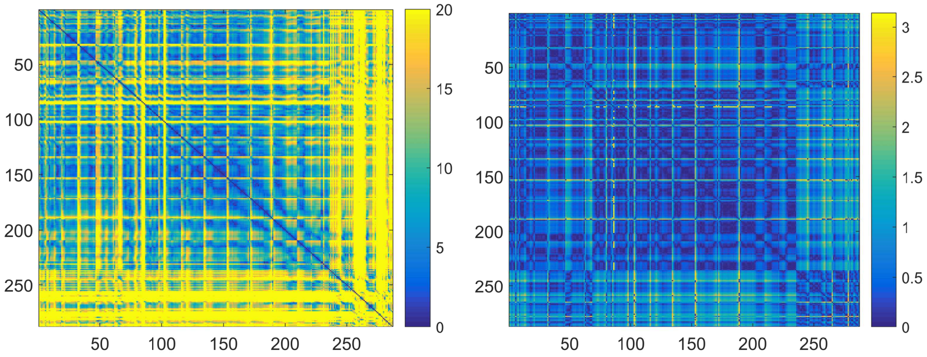

(c) $\mathbf{z}_{x,y,z}$ (d) Heading

Fig. 7. Distance matrices related to typical MF measurement models (a-c) and heading (d) for the discrete states depicted in Fig. 5. The MF distances are in μT, except for the heading, that is in radians.

standard deviation caused by the elevators is less than 5% of the total intensity, and for 2 m, it is about 2%, respectively (judging from the published graph). This is similar to results reported by Chung et al. [44]: at the distance of 1.3 m from the elevator, the RMSE in the MF intensity drops below 1 μT. The small effect of moving elevator carts is further verified by Shu et al. [58]. They measure that the effect of walking past an elevator shaft is much greater than the effect of a moving elevator cart 1 m away. Similarly, in their experiment, cars 1 m away in an underground parking lot do not have a significant effect on the magnetic intensity signal. From these results, it is quite safe to conclude that despite metallic objects affect the MF, their effect in the majority of cases is much smaller in amplitude than the variations in the indoor magnetic field caused by the static structures. This means, in practice, that even when the environment contains moving metallic objects, even in the size of elevator carts, the MF map can remain useful.

2.7 Modeling the magnetic field

As acquiring the true field is infeasible, it is approximated by an estimate $m(\mathbf{x}) : \mathbb{R}^3 \to \mathbb{R}^3$ based on a finite number of datapoints. The estimate can be modeled in a multitude of ways, differing in computational complexity and estimation error. The methods include for example piece-wise linear or bilinear interpolation [12, 13, 25, 57, 60], nearest neighbor and natural neighbor interpolation [61], and more recently, Gaussian Process (GP) [62] approaches [37, 56, 61, 63–65]. Wahlström et al. [56, 66] use GPs to model the MF based on electromagnetic theory. They are able to model the magnetic field sources and extract their properties, such as approximate shape, from the measurements. However, for localization purposes, they report only a small improvement over less-disciplined independent GP approach used, e.g., in Publication I. Solin et al. [64] improve the computational aspects of this approach by rewriting the GP model and demonstrate the model's feasibility for robotics and smartphone map generation. In his doctoral dissertation, Canciani studies modeling the MF with GPs and utilizes the GP variance in aircraft positioning [67]. GPs have also been successfully used to model the signal strength in WiFi-based SLAM [15].

2.8 Conclusions

This chapter has discussed the character of the indoor magnetic field and particularly its suitability for indoor localization purposes. Magnetic landscapes in typical modern buildings seem to have enough spatial variation to allow even sub-centimeter localization. The indoor MF is also temporally stable enough for collected maps to be usable for long periods of time. The effect of moving metallic objects is surprisingly low.

3 Recursive state estimation

3.1 Introduction

The state of the environment, especially from the robot's point of view, is not often directly observable but contains inherent uncertainty. Information is gathered by making indirect observations about the state and changing the state by moving around. As the state is uncertain, it is represented by a probability distribution over the state space.

Recursive Bayesian filtering [68] describes a principled way to recursively estimate the stochastic state when new observations are obtained and when the state changes. However, in all but few special cases, the equations in Bayesian filtering cannot be solved exactly, and approximations must be used. These include decomposing the state space into a discrete grid and making simplifying assumptions about the dynamic model.

An alternative to discretization is to recursively approximate the state probabilities numerically by an adaptive set of discrete samples, that evolves in an evolutionary-like manner based on observations, and to simulate the uncertain sample movements. These methods are called particle filters (PFs) also known as Sequential Monte Carlo (SMC) methods. They were introduced by Gordon et al. [69] in 1993. As particle filters can approximate distributions of any shape and are exceptionally easy to implement, they soon became a very popular estimation method, e.g., in mobile robotics [70] and terrain navigation [71, 72].

This chapter describes shortly the foundations of recursive state estimation and specifically particle filtering. An example of magnetic field localization with PF is given to connect the theory into practice. The theory-describing sections 3.2, 3.3, and 3.4 and their content and notation are heavily influenced by the presentations in the book *"Probabilistic Robotics"* by Thrun et al. [8] and Karlsson's PhD thesis about particle filtering [73]. An introduction to recursive Bayesian estimation can be found in a textbook by Särkkä [68] and its application to terrain navigation, e.g., in [74, 75]. Doucet et al. [76], Arulampalam et al. [77], and Tulsyan et al. [78] provide good tutorials on particle filters.

3.2 Discrete-time state space model

More often than not, the environment's state $\mathbf{x}_t$ at time t is not directly available but only observable through uncertain measurements $\mathbf{z}_t$ about the state. Numerous practical problems, such as mobile robot localization [8, 79] or aircraft or submarine terrain navigation [73, 74], can be expressed as a probabilistic discrete-time state space model, described by two stochastic processes characterized by two conditional probabilities

$$\mathbf{x}_t \sim p(\mathbf{x}_t|\mathbf{x}_{t-1},\mathbf{u}_t) \tag{3.2.1}$$

$$\mathbf{z}_t \sim p(\mathbf{z}_t|\mathbf{x}_t), \tag{3.2.2}$$

where $p(\mathbf{x}_t|\mathbf{x}_{t-1},\mathbf{u}_t)$ is called the *state transition probability* or *motion model* and $p(\mathbf{z}_t|\mathbf{x}_t)$ is called the *measurement probability* or *measurement model*. The motion model describes the probability of moving from state $\mathbf{x}_{t-1}$ to state $\mathbf{x}_t$ given control $\mathbf{u}_t$. The transition model describes the probability of observing measurement $\mathbf{z}_t$ in state $\mathbf{x}_t$.

Let $X_t = X_{1:t} = \{\mathbf{x}_1,...,\mathbf{x}_t\}$ denote an ordered set of states, $Z_t = Z_{1:t} = \{\mathbf{z}_1,...,\mathbf{z}_t\}$ ordered set of measurements, and $U_t = U_{1:t} = \{\mathbf{u}_1,...,\mathbf{u}_t\}$ ordered set of controls. In probabilistic framework, the knowledge about the environment is expressed as a probability density function $bel(\mathbf{x}_t)$, called *belief distribution* or simply *belief*. It describes a probability distribution over the states conditioned on measurements Z_t and controls U_t:

$$bel(\mathbf{x}_t) = p(\mathbf{x}_t|Z_t,U_t). \tag{3.2.3}$$

If the initial belief $p(\mathbf{x}_0)$ is known, the belief over time can be computed recursively by incorporating the most recent controls and measurements. The recursive Bayes filter derived in the next section does exactly that.

3.3 Bayes filter

In this section, the recursive Bayes update rule is shortly derived. In the following, certain assumptions about the model are made. A stochastic process is said to have the *Markov property*, if it is memoryless in the sense that if the current state $\mathbf{x}_t$ is known, past and future data are independent. This can be formulated as the *Markov assumption* (MA) about the model that consists of two parts. The first one is called *Markov property of states*, stating that if the current state $\mathbf{x}_t$ is known, the future state $\mathbf{x}_{t+1}$ does not depend on anything happened before t (3.3.1), and that also the past state

$\mathbf{x}_{t-1}$ is independent of the future states (3.3.2):

$$p(\mathbf{x}_{t+1}|X_t, Z_t, U_t) = p(\mathbf{x}_{t+1}|\mathbf{x}_t) \tag{3.3.1}$$

$$p(\mathbf{x}_{t-1}|X_{t:T}, Z_{t:T}, U_{t:T}) = p(\mathbf{x}_{t-1}|\mathbf{x}_t). \tag{3.3.2}$$

The second is called *conditional independence of measurements*. The measurements $\mathbf{z}_t$ are assumed to be conditionally independent of measurements and controls given $\mathbf{x}_t$. That is, the measurement $\mathbf{z}_t$ depends only on the current state $\mathbf{x}_t$:

$$p(\mathbf{z}_t|X_t, Z_{t-1}, U_t) = p(\mathbf{z}_t|\mathbf{x}_t). \tag{3.3.3}$$

In addition the control is assumed to be random. Further, the *Bayes' theorem* (BT) and the *Law of total probability* (LTP) are needed in the derivation. The Bayes' theorem can be written as

$$p(x|y) = \frac{p(x \cap y)}{p(y)} = \frac{p(y|x)p(x)}{p(y)}. \tag{3.3.4}$$

As the denominator $p(y)$ in (3.3.4) does not depend on x, it stays the same for all x and (3.3.4) can be rewritten as

$$p(x|y) = \eta p(y|x)p(x) \propto p(y|x)p(x), \tag{3.3.5}$$

where η is a normalization constant. Let y_i form a partition of the sample space. Then the Law of total probability for the discrete case is stated as

$$p(x) = \sum_i p(x \cap y_i) = \sum_i p(x|y_i)p(y_i). \tag{3.3.6}$$

Assume that belief $bel(\mathbf{x}_{t-1})$ from the previous time step is known. It follows from BT and measurement independence assumption (3.3.3) that

$$\begin{aligned} bel(\mathbf{x}_t) &\overset{\text{def}}{=} p(\mathbf{x}_t|Z_t, U_t) && (3.3.7)\\ &\overset{\text{BT}}{=} \eta p(\mathbf{z}_t|\mathbf{x}_t, Z_{t-1}, U_t)p(\mathbf{x}_t|Z_{t-1}, U_t) && (3.3.8)\\ &\overset{(3.3.3)}{=} \eta p(\mathbf{z}_t|\mathbf{x}_t)p(\mathbf{x}_t|Z_{t-1}, U_t). && (3.3.9) \end{aligned}$$

The rightmost distribution is called the *prediction distribution* and denoted by $\overline{bel}(\mathbf{x}_t)$. It is obtained by incorporating the most recent control u_t, but *before* using the most current measurement $\mathbf{z}_t$. The prediction distribution can be computed recursively from the previous belief, using the Markov assumption and Law of total probability

$$
\begin{aligned}
\overline{bel}(\mathbf{x}_t) &= p(\mathbf{x}_t|Z_{t-1},U_t) && (3.3.10)\\
&\overset{\text{LTP}}{=} \sum_{\mathbf{x}'} p(\mathbf{x}_t|\mathbf{x}'_{t-1},Z_{t-1},U_t)p(\mathbf{x}'_{t-1}|Z_{t-1},U_{t-1}) && (3.3.11)\\
&\overset{\text{def}}{=} \sum_{\mathbf{x}'} p(\mathbf{x}_t|\mathbf{x}'_{t-1},Z_{t-1},U_t)bel(\mathbf{x}'_{t-1}) && (3.3.12)\\
&\overset{\text{MA}}{=} \sum_{x'} p(\mathbf{x}_t|\mathbf{x}'_{t-1},\mathbf{u}_t)bel(\mathbf{x}'_{t-1}). && (3.3.13)
\end{aligned}
$$

Note that in (3.3.11), the most current control u_t could be removed from the condition set, as the controls were assumed to be random. This leads to Bayes filter recursive update rule for the discrete case, defined by the prediction (3.3.14) and the measurement update (3.3.15) steps, computed over all $\mathbf{x}_t$:

$$
\begin{aligned}
\overline{bel}(\mathbf{x}_t) &= \sum_{\mathbf{x}'} p(\mathbf{x}_t|\mathbf{x}'_{t-1},\mathbf{u}_t)bel(\mathbf{x}'_{t-1}) && (3.3.14)\\
bel(\mathbf{x}_t) &= \eta p(\mathbf{z}_t|\mathbf{x}_t)\overline{bel}(\mathbf{x}_t). && (3.3.15)
\end{aligned}
$$

The continuous case can be derived analogously, and gives update rules

$$
\begin{aligned}
\overline{bel}(\mathbf{x}_t) &= \int_{\mathbf{x}_{t-1}} p(\mathbf{x}_t|\mathbf{x}_{t-1},\mathbf{u}_t)bel(\mathbf{x}_{t-1})d\mathbf{x}_{t-1} && (3.3.16)\\
bel(\mathbf{x}_t) &= \eta p(\mathbf{z}_t|\mathbf{x}_t)\overline{bel}(\mathbf{x}_t). && (3.3.17)
\end{aligned}
$$

Given initial belief $bel(\mathbf{x}_0)$, the update rules above give the optimal solution to the recursive Bayesian estimation problem. The distributions in the continuous case are not generally available in closed form. In order to make the problem tractable, one must often rely on numerical approximations of the state space, such as dividing it into a discrete grid, or make simplifying assumptions about the state space model, such as assuming the state transition and measurement probabilities to be expressed as linear combination of Gaussians [80]. The Bayes filter can be implemented in many ways, such as point mass filters (PMF) [74], Kalman filters (KF) and its variations [80], and particle filters (PF) [77], each approximating different aspects of the problem and having different advantages and disadvantages. All Publications I-V use PF in estimation, as PF is known to perform well in multimodal environments and the magnetic environment is multimodal. Therefore, this thesis concentrates on the PF implementation presented in section 3.4.

3.4 Particle filter

Particle filter is based on the idea that the belief or *target distribution* can be recursively approximated by a large discrete set of weighted samples, called *particles*. Each particle represents a hypothesis about the state, and the *weight* or *importance factor* represents the probability of the hypothesis. The weights are computed from the mismatch between the target and the proposal distribution. As the PF approximates the densities in the Bayes filter, it provides a non-parametric approximate solution to the recursive Bayesian estimation problem. In order to concentrate the computation on areas with high probability, particles are *resampled* from time to time based on the weights. This can be thought of as an analogy to *survival of the fittest*, where each hypothesis is deemed to reproduce or perish based on its fitness (weight).

One of the main advantages of the PF is that the particles can approximate distributions of any shape. This makes it particularly suitable for environments where the distributions are multimodal and where linear or Gaussian approximations do not work [77]. The indoor magnetic field described in Chapter 2 is a good example of such multimodal environment. The multimodality is revisited later in section 3.6.4. Another important factor is that the PF is very easy and intuitive to implement. For these reasons, the particle filter has become a very popular tool for recursive state estimation, ranging from submarine and aircraft terrain navigation [71, 81] to robot localization and mapping [82, 83]. One of the main drawbacks of PF is that in high-dimensional state space, the particle density drops exponentially. This sparsity has a significant negative effect on the quality of the discrete approximation. This is known as the *curse of dimensionality* [71, 74, 84]. However, for example in mobile robot localization, the state dimension can be kept usually quite low (e.g., $d = 3$ for poses on a 2D plane).

3.4.1 Standard particle filter algorithm

Let us denote the particles as a set of P weighted samples $\mathcal{X}_t = \{\mathbf{x}_t^{(i)}\}$ and the corresponding weights as $\mathcal{W}_t = \{w_t^{(i)}\}$. The approximation $\hat{bel}(\mathbf{x}_t)$ of the belief in terms of the samples and weights can be written as follows:

$$\hat{bel}(\mathbf{x}_t) = \sum_{i=1}^{P} w_t^{(i)} \delta_{\mathbf{x}_t^{(i)}}(\mathbf{x}_t) \approx bel(\mathbf{x}_t), \tag{3.4.1}$$

where $\delta_{\mathbf{x}_t^{(i)}}(\mathbf{x}_t)$ is the Dirac delta function. The PF obtains the approximate belief $\hat{bel}(\mathbf{x}_t)$ recursively from $\hat{bel}(\mathbf{x}_{t-1})$ by applying three consecutive steps, depicted in

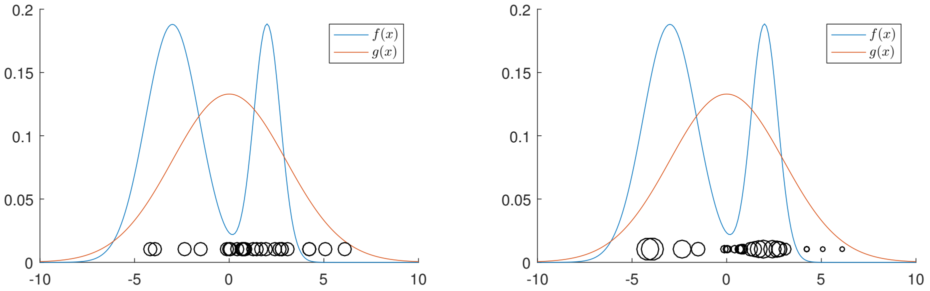

Fig. 8. Left: Samples (25) drawn i.i.d. from the proposal $g(x)$. Right: Samples weighted by $w(x) = f(x)/g(x)$ now approximate the target distribution $f(x)$. The size of the marker corresponds to the weight.

Algorithm 1, describing the Standard particle filter. First, each particle from the previous approximation $\mathcal{X}_{t-1}$ is propagated based on the motion model $p(\mathbf{x}_t|\mathbf{x}_{t-1},\mathbf{u}_t)$ (prediction, PR: in Alg. 1). Then each particle is weighted by the measurement likelihood $p(\mathbf{z}_t|\mathbf{x}_t)$ (measurement update, MU: in Alg. 1). Finally, the particles are resampled if resampling condition is met (RS: in Alg. 1). This procedure yields the samples $\mathcal{X}_t$ for the next generation.

3.4.2 Importance factor

Along with resampling, the importance factor is one of the key contributors to the basis of successful particle filtering. Let us consider two probability density functions f and g with the following properties:

- It is *difficult* or impossible to sample from f.
- It is *easy* to sample from g (e.g., Gaussian).
- Both $f(x)$ and $g(x)$ are easy to evaluate point-wise.
- $f(x) > 0$ implies $g(x) > 0$.

Function f is called the *target distribution*, and g is called the *proposal distribution*. The mismatch between f and g can be evaluated point-wise by

$$w(x) := f(x)/g(x). \tag{3.4.2}$$

The $w(x)$ above is called the *importance factor*.

Algorithm 1: Standard particle filter

```
    Input: $\mathcal{X}_{t-1}$: particles, $\mathcal{W}_{t-1}$: weights, $\mathbf{z}_t$: measurement, $\mathbf{u}_t$: control
    Output: $\mathcal{X}_t$: updated particles, $\mathcal{W}_t$: updated weights
    $\overline{\mathcal{X}}_t \leftarrow \emptyset, P \leftarrow |\mathcal{X}_{t-1}|$
PR: for $i \leftarrow 1$ to $P$ do
        draw $\mathbf{x}_t^{(i)}$ from $p(\mathbf{x}|\mathbf{x}_{t-1}^{(i)}, \mathbf{u}_t)$
        $\overline{\mathcal{X}}_t \leftarrow \overline{\mathcal{X}}_t \cup \mathbf{x}_t^{(i)}$
    end
    $\mathcal{W}_t \leftarrow \emptyset$
MU: for $i \leftarrow 1$ to $P$ do
        $w_t^{(i)} \leftarrow p(\mathbf{z}_t|\mathbf{x}_t) w_{t-1}^{(i)}$
        $\mathcal{W}_t \leftarrow \mathcal{W}_t \cup w_t^{(i)}$
    end
    $\mathcal{W}_t \leftarrow$ normalize($\mathcal{W}_t$) to sum to 1
    $\mathcal{X}_t \leftarrow \emptyset$
RS: if doResample then
        while $|\mathcal{X}_t| \leq P$ do
            draw $\mathbf{x}'$ from $\overline{\mathcal{X}}_t$ proportionally to $\mathcal{W}_t$
            $\mathcal{X}_t \leftarrow \mathcal{X}_t \cup \mathbf{x}'$
        end
        foreach $w_t^{(i)} \in \mathcal{W}_t$ do
            $w_t^{(i)} \leftarrow 1/P$
        end
    else
        $\mathcal{X}_t \leftarrow \overline{\mathcal{X}}_t$
    end
    return $\mathcal{X}_t$, $\mathcal{W}_t$
```

Let us examine the probability that x falls inside a interval A. This probability is $f(x \in A) = f(A)$, and through expectation, it gives a relation between $f(A)$ and $g(A)$:

$$\begin{aligned}
f(A) &= E_f[\delta_x(A)] && (3.4.3)\\
&= \int f(x)\delta_x(A)dx && (3.4.4)\\
&= \int \frac{f(x)}{g(x)} g(x)\delta_x(A)dx && (3.4.5)\\
&= \int w(x)g(x)\delta_x(A)dx, && (3.4.6)
\end{aligned}$$

where $\delta_x(A)$ is the Dirac measure. If g is approximated by discrete samples $\{\mathbf{x}_t^{(i)}\}$, then $f(A)$ can be approximated by weighting each sample with point-wise evaluated *importance factor* $w_t^{(i)} = f(\mathbf{x}_t^{(i)})/g(\mathbf{x}_t^{(i)})$:

$$\begin{aligned}
f(A) &= \int w(x)g(x)\delta_x(A)dx && (3.4.7)\\
&\approx \eta \sum_{1}^{P} f(\mathbf{x}_t^{(i)})/g(\mathbf{x}_t^{(i)})\delta_{\mathbf{x}_t^{(i)}}(A) && (3.4.8)\\
&= \eta \sum_{i=1}^{P} w_t^{(i)} \delta_{\mathbf{x}_t^{(i)}}(A), && (3.4.9)
\end{aligned}$$

where $\eta = 1/\sum w_t^{(i)}$ is a normalizing factor. Therefore, the target function f can be approximated by the weighted sum of the particles drawn from the proposal g:

$$f(x) \approx \eta \sum_{i=1}^{P} w_t^{(i)} \delta_{\mathbf{x}_t^{(i)}}(x) = \hat{f}(x). \tag{3.4.10}$$

It can be shown that the empirical probability of $x \in A$ converges to $g(A)$, when $P \to \infty$:

$$\hat{g}(x) = \frac{1}{P} \sum_{i=1}^{P} \delta_{x^{(i)}}(A) \longrightarrow \int_A g(x)dx. \tag{3.4.11}$$

Further, it can be shown that the weighted approximation $\hat{f}(A)$ converges to $f(A)$:

$$\hat{f}(x) = [\sum_{i=1}^{P} w^{(i)}]^{-1} \sum_{i=1}^{P} w^{(i)} \delta_{\mathbf{x}^{(i)}}(A) \longrightarrow \int_A f(x)dx. \tag{3.4.12}$$

A survey of PF convergence results can be found in [85]. In particle filtering, f corresponds to target belief $bel(\mathbf{x}_t)$ and g usually corresponds to the proposal $p(\mathbf{x}_t|\mathbf{x}_{t-1}, \mathbf{u}_t) = \overline{bel}(\mathbf{x}_t)$, as the proposal is easy to sample from. In this case, f/g corresponds to the measurement likelihood:

$$\frac{\eta p(\mathbf{z}_t|\mathbf{x}_t)\overline{bel}(\mathbf{x}_t)}{\overline{bel}(\mathbf{x}_t)} \propto p(\mathbf{z}_t|\mathbf{x}_t) \tag{3.4.13}$$

computed in the measurement update of Algorithm 1. A particle filter with this particular choice is known as the *bootstrap filter* [69].

3.4.3 Motion model

In mobile robotics, the transition model $p(\mathbf{x}_t|\mathbf{x}_{t-1},\mathbf{u}_t)$ is called the *motion model*. In PF, this is implemented by simulating the robot's motion by drawing samples from the motion model and then propagating the particles accordingly (see, Algorithm 1 PR:). The motion models in this thesis consider a robot operating on a plane, i.e., $\mathbf{x}_t = (x_t, y_t, \theta_t)^T$, that receives a control $\mathbf{u}_t = (x'_t, y'_t, \theta'_t)^T$. A very simple motion model $\mathbf{x}_t = \mathbf{x}_{t-1} + \mathbf{u}_t + e(\mathbf{u}_t)$ for such robot can be described as

$$x_t = x_{t-1} + x'_t + e_x(u_t) \tag{3.4.14}$$

$$y_t = y_{t-1} + y'_t + e_y(u_t) \tag{3.4.15}$$

$$\theta_t = \theta_{t-1} + \theta'_t + e_\theta(u_t), \tag{3.4.16}$$

where e_i are errors depending on the control and the robot motion dynamics [86]. Propagating particles with this kind of model are illustrated in Figure 10, and an example of mobile robot localization using such a model is given in section 3.6.

3.4.4 Measurement model

For the purposes of this thesis, the measurement model $p(\mathbf{z}_t|\mathbf{x}_t)$ is considered for measurements consisting of the magnetic field vector $\mathbf{z} = (z_x, z_y, z_z)^T$. In the literature [41, 43, 45], magnetic measurement models are based basically on three different vectors extracted from the measurement vector z, discussed more thoroughly in section 2.5: norm of the vector $||\mathbf{z}||$, yaw-independent vector $\mathbf{z}^\perp = (||\mathbf{z}_{x,y}||, z_z)^T$, and full vector $\mathbf{z}$. The distinctiveness of the vectors is illustrated in Figure 7. The likelihood function can be for example a Gaussian

$$p(\mathbf{z}_t|\mathbf{x}_t) = \eta \exp\left(\frac{-d(\mathbf{z}_t, m(\mathbf{x}_t))^2}{2\sigma^2}\right), \tag{3.4.17}$$

where η is a normalization factor, $d(\mathbf{z}_, m(\mathbf{x}_t))$ is a distance between the measurement and estimated measurement in the map, and σ^2 is the variance capturing, e.g., map estimation errors and measurement noise. Euclidean and Manhattan distances are found to give similar results [41]. This kind of measurement model is used in the example in section 3.6. Not surprisingly, the full vector, when applicable, has been found to provide the best results, as it is able to distinguish the different orientations of the sensor with respect to the MF [41, 45, 87]. Other possible three-component vector representation is to use $\mathbf{z}^{\perp}$ with the full vector's heading on the horizontal plane. This allows more control over heading likelihood, although in the rare case when $\mathbf{z}_{x,y}$ is close to zero it may be sensitive, e.g., to noise.

An alternative for using the full vector is to use independent likelihood functions for each channel. This can be done to model, e.g., the outlier distribution for each channel separately, possibly making the model more robust to channel-wise bias and noise. Another advantage is the possibility to tune the parameters, e.g., variance, for each channel separately. This approach was taken in Publications I and II, where channels were given different variances based on learned data and the likelihoods were modeled as a mixture of a Gaussian and uniform distribution.

An important note about the measurement model is that although single measurements are often not able to determine the place unambiguously, as can be seen, e.g., from the MF distance matrices in Chapter 2, the recursive multiplicative weight update will very quickly discriminate between paths even in the presence of noise. Robertson et al. [88] make an analogy to communications theory, where single observations about the field intensities correspond to code symbols and sequences of observations correspond to code words, whose distance to competing words grows with the word length.

3.4.5 Resampling

Without the resampling step, the particle weights would soon become very unevenly distributed, and eventually all but one particle would have negligible weights. This problem is known as *particle depletion* and it is tackled by the resampling step introduced by Gordon et al. [69]. In resampling, particles with small weights are replaced with copies of particles with high weights, after which the weights are set uniform. This guides the particle approximation to regions with high probability. As the selection is done proportional to the particle weights, the resulting particle set with uniform weights still approximates the posterior [89]. If the particle-based filtering is done without the resampling step, the algorithm is known as *sequential-importance-sampling* (SIS), and if resampling is performed (every step or adaptively), it is known as *sequential-importance-resampling* (SIR) [77, 90]. The resampling is often done by roulette wheel selection, i.e., drawing particles with replacement based on the distribution defined by the particle weights. Alternative resampling techniques, such as residual and systematic resampling, exist as well. They have been shown to produce samples with less sampling variance and more efficiently [91, 92], therefore being superior to i.i.d. sampling in most practical cases.

3.4.6 Estimates and density extraction

It is often enough to obtain a single point estimate from the particle representation of the belief. The most commonly used one is the *minimum mean square* (MMS) estimate that is obtained directly by computing the weighted mean of the particles

$$\hat{\mathbf{x}}_t^{MMS} = \sum_{i=1}^{P} \mathbf{x}_t^{(i)} w_t^{(i)} \tag{3.4.18}$$

that minimizes the sum of squared differences from the mean. Other alternatives include, e.g., the *maximum a posteriori* (MAP) estimate that is simply the particle with the highest weight [73]. Sometimes, however, one wants to turn the particles into a density representing the belief. In unimodal case, a Gaussian approximation is often adequate. For multimodal cases, the density can be extracted, e.g., using histogram approximations or kernel density estimation, where each particle is replaced, e.g., by a Gaussian kernel. The kernel densities are then summed to obtain the final density. Examples of densities obtained by both methods are visualized in Figure 9. It should be noted that the estimation using any of these methods should be done before resampling, as resampling introduces additional randomness in the current approximation [89]

3.5 Sampling variance

The sampling in Monte Carlo approximations introduces additional random error to the approximation, caused by sampling variance. This affects both resampling and prediction steps in the PF algorithm. For example, in resampling, especially with i.i.d. roulette wheel sampling, particles with significant weight can be chosen to be randomly replaced. This so-called *sample impoverishment* causes similar effect to particle depletion, where the posterior is approximated only a small number of (copied) samples [77]. One way to tackle this is to reduce the variance in the resampling step. This can be done by selecting the surviving particles more systematically. Examples of such resampling schemes are Residual Resampling and systematic sampling [89, 91, 92].

Another way to reduce the error caused by resampling is to use an adaptive resampling scheme, where the resampling step is only taken when there is enough variation in the particle weights. The *effective sample size* [89] can be approximated using the variance of the normalized weights

$$N_{eff} = \frac{1}{\sum (w_t^{(i)})^2}. \tag{3.5.1}$$

This ranges from 1 to N, and can be thought of as the number of particles contributing significantly to the posterior. It has been shown to decrease stochastically over time [93]. Adaptive resampling based on N_{eff} has become the standard approach [8, 94]. For example, a predefined threshold $N_{eff} < P/2$ can be used to decide if to carry out the resampling step in the Standard particle filter (Algorithm 1).

The other step introducing sampling variance is the prediction step. This is discussed in section 3.5.1.

3.5.1 Improving the proposal approximation

In optimal situation, the proposal would be directly replaced by the so-called *optimal importance density* $p(\mathbf{x}_t|\mathbf{x}_{t-1}^{(i)}, \mathbf{z}_t)$, as it minimizes the variance between the importance weights [93]. However, using it is not generally possible, and usually if one wants to improve the proposal, approximations must be used. Traditionally, in robotics, the proposal distribution is improved by reducing the mismatch between the proposal and the posterior in order to get away with a small number of particles. The number may be constrained, e.g., due to memory constraints caused by large occupancy grid maps [94–96]. When the number of particles is low, it is crucial that the samples drawn from the proposal end up in areas with high likelihood [77, 89]. There are many approaches to this problem. Grisetti et al. achieve this by adapting the proposal by utilizing the most recent laser range measurement [96], and Grzonka et al. use look-ahead particles to peek into the future to produce an improved proposal to cope with feature-poor environments [97]. Both approaches improve the PF performance considerably. However, even when such an approach is not possible, e.g., when information about the posterior is not available [98], the proposal approximation can be improved by decreasing the sampling variance. This can be achieved, e.g., by generating the proposal-approximating samples

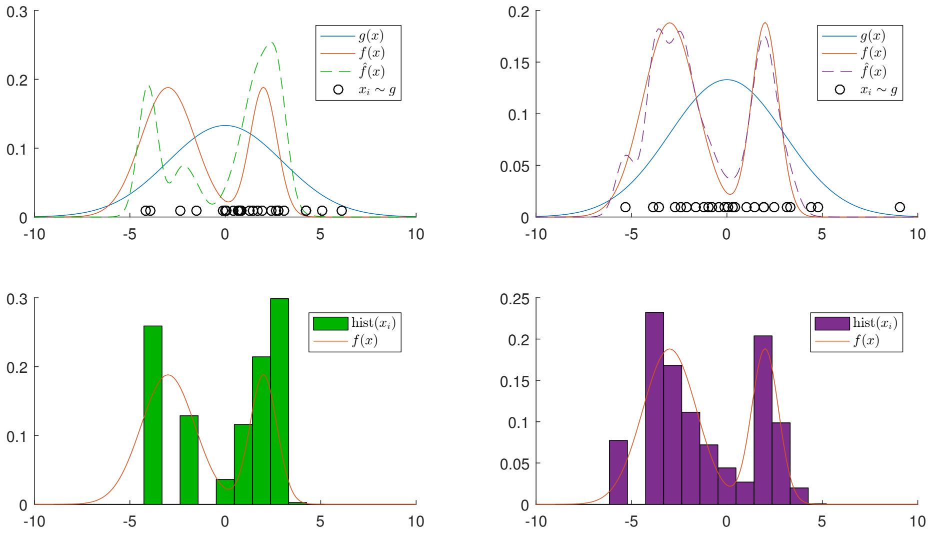

Fig. 9. Density extraction from the approximated posterior visualizes the possible negative effect of sampling variance (left column) and how it can be alleviated by systematic sampling (right column). The top row illustrates the 25 samples x_i drawn both i.i.d. (left) and systematically (right) from the proposal $g(x)$ and the approximation $\hat{f}(x)$ as a sum of weighted Gaussians. The bottom row illustrates a histogram approximation.

systematically as evenly as possible instead of using i.i.d. sampling. The method is also known as *quasi-random sampling* [99], and it is proven to lower the error rate of the particle filter [98, 100, 101].

Publication IV introduces Systematic Alias Sampling (SAS) as a way to produce low-variance samples very effectively from an arbitrary discrete distribution. SAS is based on the idea of combining the alias method by Walker [102] and systematic sampling used widely in robotics [77]. Figure 9 illustrates how i.i.d. sampling procedure may produce samples ($P = 25$) that represent the proposal g very badly. As a consequence, the approximation $\hat{f}$ of the posterior f is also very poor. The figure illustrates densities extracted from the samples both as a sum of weighted Gaussians ($\sigma^2 = 1^2$) and also as a histogram. Figure 10 illustrates the same phenomenon in the context of motion model. Two particle filters with 50 particles, depicted in blue (i.i.d.) and red (SAS), are compared w.r.t. the mean estimate of a filter with 5,000 particles (grey). The left side illustrates the simulated proposal for six consecutive steps with the corresponding mean estimates, and the right side depicts the difference to the PF with 5,000 particles over 20 similar steps. Again, systematic sampling estimates the proposal better. Systematic

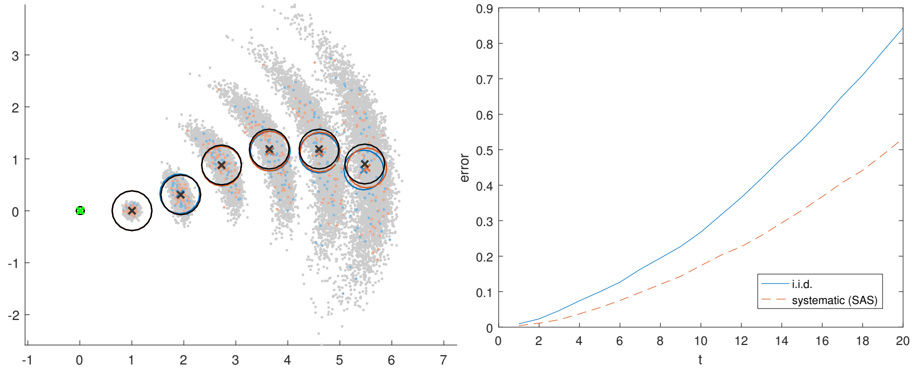

(a) (b)

Fig. 10. The effect of sampling variance to sampling from a motion model. (a): Two sets of 50 particles (blue, red) are propagated for six steps with different sampling strategies (i.i.d. and systematic). The weighted average is compared to average of a 5,000 particle set (grey). (b): The difference for 20 time steps averaged over 30 runs.

sampling in the motion model is especially beneficial when the majority of particles have converged to a single point. Ormoneit et al. [100] construct an example case where i.i.d. sampling in motion model fails with high probability. Systematic samples for both illustrations are generated with SAS by using a 1009-valued approximation of the normal distribution (see, IV for details).

3.6 Example: Monte Carlo localization on the magnetic landscape

In robotics, localization using a particle filter is often called Monte Carlo Localization (MCL) [79, 82]. Using an illuminating example, this section shows that a magnetic field map contains enough information to be used for localization. A particle filter is used to localize and track a robot using only noisy control commands and noisy magnetometer readings. The localization presented here is very close to terrain navigation on magnetic landscape by Solin et al. [103] that uses a mobile device carried by human to perform a similar localization task. The environment is the University of Oulu Discus Lobby presented in Chapter 2. A grid map of the magnetic landscape with resolution of 0.2 m is collected beforehand and considered known. The robot follows a random spline trajectory X_t' depicted as a green dashed line in Figure 11. The state of the robot is estimated using the standard particle filter described in Algorithm 1 with $1,000$ particles and the following parameters.

3.6.1 Controls and Motion model

The controls are in form $\mathbf{u}_t = (x_t, y_t, \theta_t)^T$, representing a translation (m) followed by a rotation (rad). The controls are given in approximately 20 cm interval, as 250 consecutive segments of a polyline approximating the spline trajectory. The control components are derived from the segments $\mathbf{u}'_t = (x'_t, y'_t, \theta'_t)^T$ of the true trajectory and are affected by the following random error terms:

$$x = x'_t + 0.2\, x'_t\, e_1 \tag{3.6.1}$$

$$y = y'_t + 0.2\, y'_t\, e_2 \tag{3.6.2}$$

$$\theta_t = \theta'_t + 0.2\ \theta'_t\ e_3 + 0.002\ (|x'_t| + |y'_t|)\ \pi\ e_4, \tag{3.6.3}$$

where e_i are drawn from the standard normal distribution. The error terms depend mainly on the corresponding element, but the angular term also has a cross-component that is affected by the translational elements in the control. For the sake of simplicity, the error model is assumed to be known and it is used directly to propagate the particles.

3.6.2 Measurements, Measurement model, and Resampling

The measurements $\mathbf{z}_t = m(\mathbf{x}'_t) + e_{\mathbf{z}}$ are generated by the nearest neighbor interpolation from the MF map by rotating the interpolated values around z-axis based on the simulated poses in the trajectory X'_t. In addition, independent Gaussian noise $e_{\mathbf{z}}$ with $\sigma = 3$ (μT) is added to each channel. The true and noisy signals are depicted in Figure 12 (a). The measurement model is defined as a Gaussian

$$p(\mathbf{z}|\mathbf{x}) = \eta \exp\left(\frac{-d_1(m(\mathbf{x}), \mathbf{z})^2}{2\sigma_z^2}\right), \tag{3.6.4}$$

where $\sigma_{\mathbf{z}}^2 = 10^2$ and $d_1(m(\mathbf{x}), \mathbf{z})$ is the Manhattan distance between the map value in pose coordinates and the measurement. Using Euclidean distance with scaled variance should yield similar results [41]. Resampling is performed only when N_{eff} drops below $P/2$. The particles are resampled using the Residual Resampling [89].

3.6.3 Localization along a simulated trajectory

A standard particle filter with the given parameters and input is used to estimate the traveled trajectory. The particles are initialized uniformly on the map. The localization

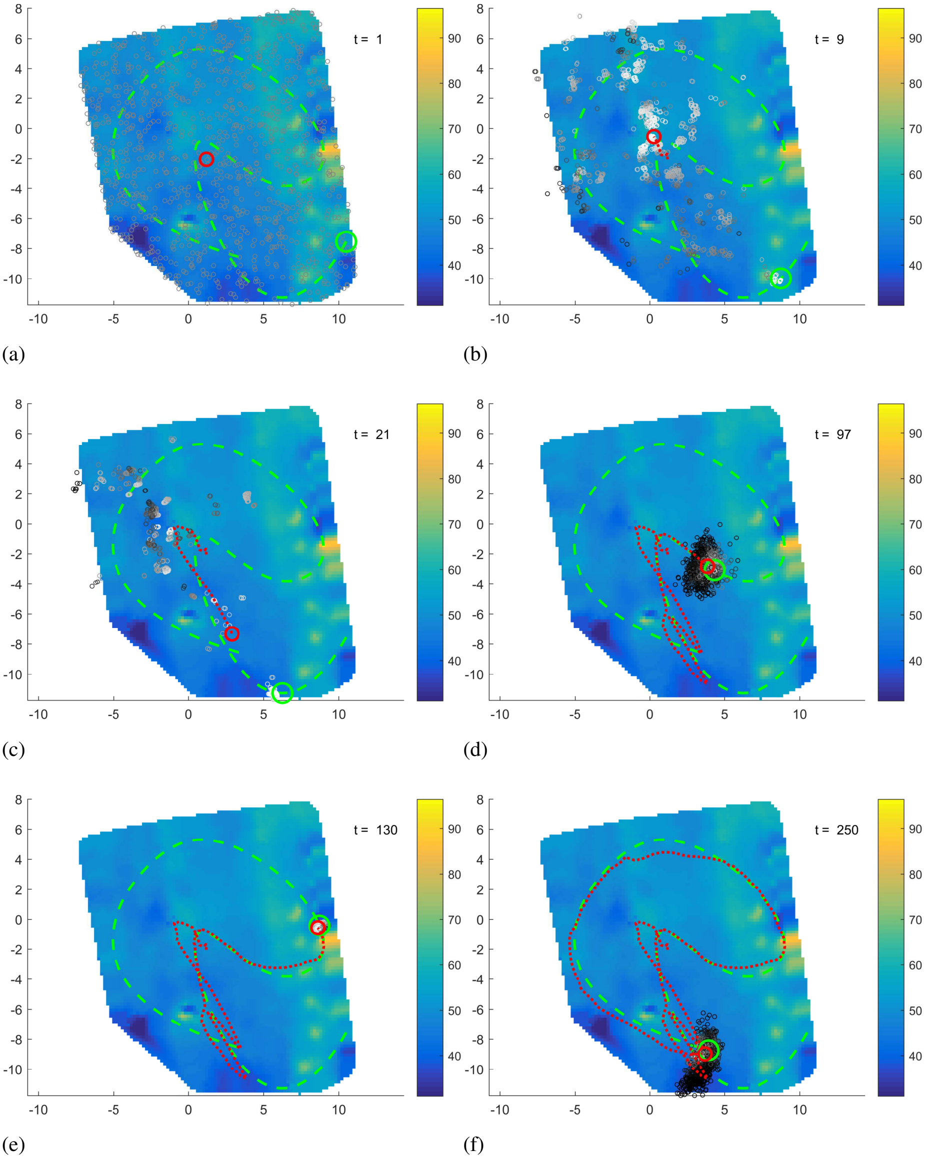

(a) (b) (c) (d) (e) (f)

Fig. 11. Snapshots from different time steps of MF-based simulated MCL experiment superimposed on the MF magnitude map (μT). Green circle and dotted line represent the true location and path, respectively. Estimated pose and path are depicted in red. Particles are in shades of gray, where shades toward white represent high weight.

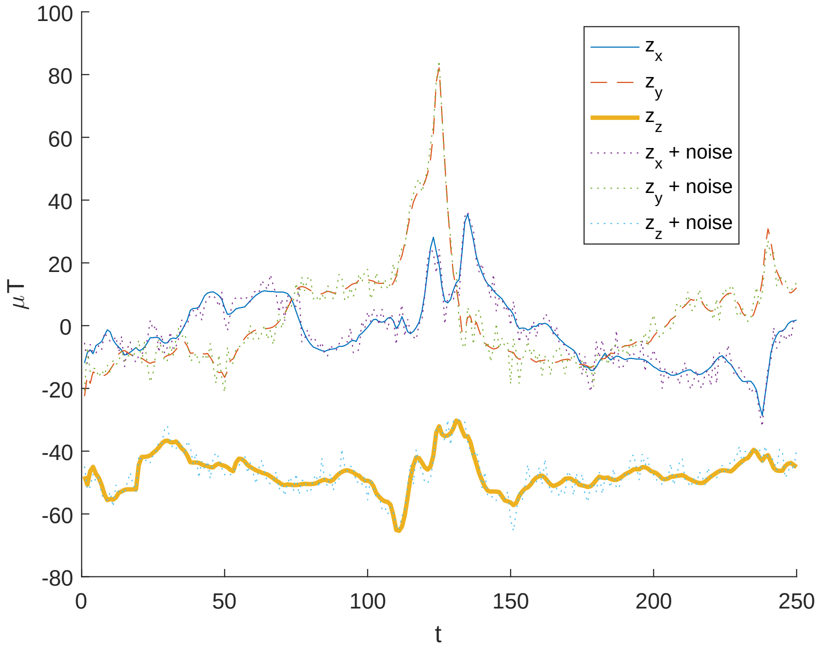

(a) Magnetic measurements along the path.

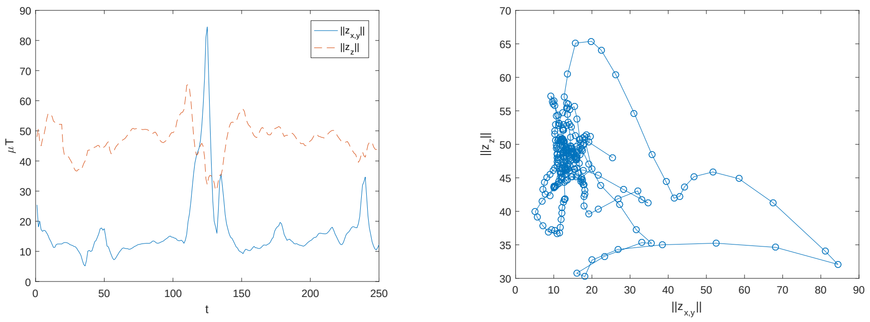

(b) The norms of the horizontal and vertical components.

(c) Walk of the norms of horizontal and vertical components. The intersections reveal the inherent multimodality.

Fig. 12. Visualization of the magnetic data over the path used for localization

is illustrated in Figure 11. The true trajectory and pose are depicted in green, particles in shades of gray (light color meaning high weight), and weighted mean estimate and its path in red. Initially, the particles are distributed evenly in the state space (a). As the robot moves, the particles start to concentrate to multiple modes due to PF update (b-c). Finally, only the true mode is left (d). Distinct features in the MF concentrate the particles very tightly (e). More flat regions make the cloud disperse but still stay easily on track (f). As can be seen, the particle filter is able to both converge to the true location and after that track the trajectory of the robot.

3.6.4 Note on multimodality - signal as a random walk

Figure 12 (c) depicts the walk of $\mathbf{z}_t^{\perp} = (||\mathbf{z}_{x,y}||, z_z)_t^T$ in $\mathbb{R}^2$. Despite the robot trajectory intersects itself only once at the very end (Fig. 11), it can be seen that $\mathbf{z}_t^{\perp}$ intersects itself very often. This means that, if the heading is not known, there are multiple locations with an identical magnetic field, even along the measured path. With no information about the indoor MF, when the signal is collected along a continuous path, it is reasonable to think of $\mathbf{z}_t^{\perp}$ as a continuous random walk in 2D that is (physically) constrained more or less around the mean (Earth's MF). Generally, even non-constrained random walks in 2D tend to intersect, as for both simple random walks and Brownian motion, the probability for non-intersecting paths has exponential decay [104], with the exception of an exponentially small number of self-avoiding walks [105]. Furthermore, it has been proven that for a certain type of continuous n-step random walk, the expected number of self-intersections is asymptotically $(2/\pi^2)n\log n$ [106, 107]. Empirical data visualized in Figure 12 (c) clearly suggests that MF signal as a random walk does not seem to be an exception and highlights the inherent multimodality present in MF localization. This is not surprising, as there is no reason to assume a self-avoiding property in the MF signal.

3.7 Conclusions

This chapter has provided the building blocks for MF-localization using a particle filter to obtain an approximate solution to the Bayesian filtering problem. The solution is visualized with a concrete example in MF-localization. Additionally, some improvements in the motion model sampling procedure have been discussed as well.

4 Magnetic field navigation and localization

4.1 Introduction

Magnetic field localization is closely related to MF-SLAM. The main difference is that in localization, the map of the environment is assumed to be known. This chapter provides a short description of the early work and methods most commonly used in the field. For details, the reader is referred to the literature provided.

Traditionally, compasses and magnetometers have been used to estimate the compass heading that is used, e.g., for robot localization or gyroscope drift correction in IMU-based approaches. In many cases, the magnetic disturbances caused by the ferromagnetic structures inside the buildings have been seen as erroneous readings that must be compensated or at least detected and ignored [108–112]. Sometimes, the magnetic anomalies are seen completely adversary to localization and impossible to estimate [113], as it corrupts the "correct" compass heading for foot-mounted IMU purposes. Sometimes even the magnetic map is collected in order to get corrected compass readings [57]. Beginning from seminal work by Haverinen et al. [1] in 2008, a gradual paradigm shift begun in which the anomalies are seen as a source of information for localization rather than an error.

The most popular indoor localization techniques in the robotics literature are based on range sensors. Laser-based localization has long provided very accurate estimates in controlled and static environments, and even ultrasonic sensors provide accuracy that is good enough for many practical settings. However, there are many real environments with features that have been proven difficult, e.g., for laser-based localization. For example, windows or walls made of glass, very small objects, smoke, and crowded, dynamic environments all pose hurdles for the localization [114–116].

One way to overcome these obstacles is to design algorithms that are able to handle the difficult and unambiguous sensor readings. Another way is to use sensor fusion to incorporate information from other sensors to reduce the overall uncertainty. Magnetic field measurements have been used for this purpose in conjunction with range and radio-based measurements in several papers [109, 117–120]. The main advantage of using magnetic field sensors is that the measurements are usually very weakly correlated with measurements provided by other sensors, and therefore, the magnetic field can be used to derive independent information about the surroundings. For example in [118], magnetic field measurements are used with laser-based localization to aid in global localization after robot kidnapping.

4.2 Magnetoreception in animals

Many animals, from insects to vertebrates, are known to have magnetoreception, i.e., they are able to detect the Earth's magnetic field [121, 122]. The animals utilize the Earth's magnetic field for either navigation or other purposes, such as orientation detection [123]. The species that are known to navigate via magnetoreception include migratory birds [124, 125], bats [126], salmon [127], marine turtles, and spiny lobsters [128, 129]. Many insects, such as hornets, ants and termites [130–132], utilize the magnetic field to orient themselves for example when building the nest, and disturbed magnetic field, e.g., near power lines, may lead to nest structures aligned with the magnetic field. The exact method of how the animals sense the magnetic field is still unknown. Many competing theories have been proposed to explain the nature of magnetoreception [121]. In a very recent study, the authors were able to identify an iron-containing protein spontaneously aligning in the magnetic field that is possibly responsible for the magnetic sensing [133].

4.3 Early work

As such, the idea of using the variation in the Earth's magnetic field for tracking and navigation is not new. In 1982, Tyrén [134] suggests that the variation could be used as a basis for ground-speed estimation for vehicle and aircraft localization and later describes a navigation system for submarines that utilizes the underwater magnetic field anomalies to track the vehicle [135]. The undergraduate report by McKay et al. [136] in 1998 is the first study of which the author is aware of where the indoor magnetic field disturbances are used to localize a mobile robot. The paper describes a robotic mapping system, where the robot collects compass data on predefined coordinate nodes and later utilizes the disturbance signature to localize the robot to the best matching node. The system achieves about one meter accuracy in small environments and near walls, where there is enough variation in the magnetic landscape. Probably due to the immaturity of the mobile robot localization and mapping at the time, the promising preliminary results were not taken further. With very few exceptions, the next studies on the subject begun to surface almost ten years later, e.g., after particle filters were widely adopted in mobile robotics localization research [16, 47].

One of the earliest works utilizing a magnetic field disturbance map is by Suksakulchai et al. [49] in 2000. The robot is manually driven along corridors to collect the map and the local headings are recorded using an electronic compass. These deviations from the compass direction are then used to perform robot localization. The localization method considers a moving window of measurements and is based on minimizing the least squares problem between the measurements and the map reference. The method achieves corridor-level accuracy.

In the work starting at 2008 Haverinen et al. [1, 16, 137] suggest that the indoor magnetic field could be used as a signal for localization purposes. They describe the first modern solution to indoor magnetic field localization and mapping. The magnetic field is measured along corridors to produce one-dimensional magnetic signal maps. Localization is performed using an SIR particle filter and the norm of the measurements, as the orientation of the sensor is not available. Experiments in multiple buildings for both robot and wearable sensor show that the magnetic field is temporally stable and indeed usable for indoor localization purposes, achieving mean estimation errors from 0.1 m (robot) to 3.5 m (wearable sensor). The applicability of the method is later verified also in underground mines [87].

In 2009, Rahok et al [138] describe a system to correct errors in robot odometry using the variations in the indoor magnetic field. Map of the three-component magnetic vector is collected and the robot is localized along a rectangular trajectory in a small environment (0.75×6.0 m^2) using vision-based wall-following system that is able to keep the robot's distance from walls constant. Sub-decimeter estimation error is obtained.

4.4 Localization methods

Magnetic field localization is in many ways similar to terrain navigation, that has been used to track submarines and aircraft based on the terrain elevation maps [74, 75, 139, 140]. If only the norm of the magnetic field is used, as in many papers [60, 118, 137, 141], the magnetic landscape is very similar to the terrain height map. If more components of the measurement vector are used, also directional information can be utilized [25, 41, 43, 45, 103]. Some of the early work rely solely on the heading information [49, 57]. Due to similarities to terrain navigation, similar methods, such as

PFs, are applicable also to MF navigation [25, 42, 103, 118, 137]. When the trajectories can be restricted to one-dimensional paths, e.g., in the middle of corridors, also methods such as dynamic time warping can be used [53, 142, 143]. Also Kalman filters are used in some of the research [47, 144].

4.5 Magnetic field map model

Modeling the magnetic field ranges from detecting and modeling clear landmarks, such as elevators and pillars [54, 55, 145], or detecting room-level signatures [146] to interpolating raw data on a grid [16, 25, 57, 60] or using Gaussian mixture models [147]. More recently, the magnetic field has been modeled for localization purposes using sophisticated physics-based Gaussian Process models to deal with sparse data and model the associated uncertainties [63, 65–67, 103, 117]. Most of the research depends on the natural magnetic variation, but in some work, artificial fields are induced using magnetic coils with known properties [65, 144, 148].

4.6 Mobile devices

Almost all modern mobile devices have a multitude of sensors, including an accelerometer, gyroscope, and magnetometer. This has made the MF localization possible using smartphones in indoor environments, where GPS is not available. This offers business opportunities in the indoor location market [18, 29]. The early ideas from robotics were soon adopted to mobile devices [25, 55, 103, 117, 149, 150]. Gozick et al. [55] propose the first approach to build indoor magnetic maps using smartphones. In their approach the map consists of magnetic landmarks, such as elevators and steel pillars, that are shown to provide temporally stable and device-independent features in the norm of the magnetic field that can be used for localization. LeGrand et al. [25] manually collect a non-parametric dense 2D grid map of the magnetic field using the full three-component magnetic field vector. It is demonstrated how the map can be used to localize a smartphone with 0.7 m accuracy. Torres-Sospedra et al. [24] provide benchmark data sets for both WiFi and MF-based indoor localization.

An accelerometer can detect the direction of gravitation, so the magnetometer reading can be rotated to the horizontal plane [48]. If we assume the mobile device is held approximately at constant height and localize with respect to the mobile device coordinates, the situation becomes similar to the 2D mobile robot case, as only the planar coordinates and heading need to be estimated. In general, however, the magnetic field localization on mobile devices is much harder. For example, the sensor height, orientation, and movement must be estimated. In addition, possible dynamic sensor biases due to the device's physical electrical and metal components must be accounted [47]. On dedicated platforms, such as mobile robots, one can position the magnetometer away from the platform's electrical and metal components, thus minimizing interference [42, 64, 137]. On consumer-grade electronics, such as smartphones and tablets, this is not often feasible, as the sensors are embedded inside the device. For example, the changing CPU load can cause electromagnetic inference to the MF readings, and a metal casing may introduce a constant bias. These usually do not pose problems for the average developer, as typical uses for compass heading and inertial measurement unit (IMU) are fairly robust to these kind of changes, and, e.g., Android API provides automatically bias-corrected sensor readings. On the other hand, the gap between consumer-grade sensors and the sensors that have been used in research, is closing, and the manufacturers are reacting to the need of high-quality sensor data. As from Android API level 20 (2014), the developer has been able to request also raw, uncalibrated magnetometer readings to be used for custom calibration. To mitigate the sensor power consumption problem, Google introduced The Android Sensor Hub (2015) on a few selected mobile phone models. It is a dedicated low-power processor used on mobile devices to exclusively handle sensor data relieving the main CPU from the task, dropping power consumption to only a fraction of current consumption.

4.7 Conclusions

During the last fifteen years the variations in indoor magnetic field have gone through a paradigm shift from a source of errors to source of information. Magnetic field-based indoor localization is an active research field in both robotics and mobile device context. With improving sensor technology on consumer-grade devices, magnetic field based localization is becoming one of the most promising solutions to take the place of the "indoor-GPS".

5 Simultaneous localization and mapping

5.1 Introduction

The map of the environment is not always readily available, and the agent (human or robot) has to come up with a map on its own during the localization. This is called the *simultaneous localization and mapping* (SLAM) problem. It was first introduced by Smith et al. [151]. It is considered one of the most fundamental problems in the mobile robotics literature [8, 9]. SLAM is often described as a chicken-egg problem [8]. On the other hand, it can also be considered as a sequence of localization problems with very poor or virtually non-existent maps – problems that (hopefully) become progressively easier as the mapping continues. The main goal is to properly maintain the very uncertain distribution over the trajectories until the localization becomes unambiguous. In robotics the measurements traditionally come from a laser range finder. The problem has been tackled with particle filters [96] and more recently via graph-based (GraphSLAM) approaches [152]. At first, the occupancy grid-based SLAM problem was tackled with a PF with only a single map [153]. The introduction of *Rao-Blackwellized particle filter* (RBPF), where each particle carries its own map, improved the results significantly. RBPF for grid maps was first introduced by Murphy [154] and Doucet [93]. It was later improved to handle large environments with high resolution [83, 94, 155, 156]. Montemerlo et al. [157] provide an RBPF solution to large scale landmark-based SLAM. Cadena et al. [9] give a very recent (2016) survey on current state and future directions of SLAM. It also briefly discusses the use of non-traditional sensors.

As early as 1987, Tyren [135] suggested underwater magnetic field SLAM in the form of gradual map enlarging. However, as far as the author knows, Publications I and II were the first ones daring to tackle the indoor SLAM problem using only the magnetometer readings along with odometry. Since then, magnetic field-based SLAM or more shortly MF-SLAM has quickly become an active research topic [13, 27, 88, 118, 158–160]. After introducing the theory behind MF-SLAM methods in Publications I - II and V, the most relevant research on MF-SLAM is shortly reviewed in section 5.5.

5.2 Rao-blackwellized particle filter

The idea of Rao-Blackwellised particle filter is to estimate the joint posterior $p(X_t, m_t|Z_t, U_t)$ of the trajectory of poses X_t and the map m_t conditioned on the observations Z_t and controls U_t. Under the assumption that the map does not depend on the control if the poses and measurements are known, the following factorization of the joint posterior is obtained:

$$p(X_t, m_t|Z_t, U_t) = p(m_t|X_t, Z_t, U_t)p(X_t|Z_t, U_t) \tag{5.2.1}$$

$$= \underbrace{p(m_t|X_t, Z_t)}_{\text{map}} \underbrace{p(X_t|Z_t, U_t)}_{\approx \mathcal{X}_t}. \tag{5.2.2}$$

The right side can be recursively approximated by a particle filter. For each particle, the map can be built analytically from the poses and the measurements, also known as *mapping with known poses* [83]. In other words, each particle $\mathbf{x}_t^{(i)}$ carries its own map $m_t^{(i)}$, and the measurement update for the PF becomes

$$w_t^{(i)} = p(\mathbf{z}|\mathbf{x}_t^{(i)}, m_{t-1}^{(i)})w_{t-1}^{(i)}. \tag{5.2.3}$$

Map $m_t^{(i)}$ for each particle is then computed (or updated) analytically based on the trajectory $X_t^{(i)}$ and the measurements Z_t. Particle filter utilizing the above factorization is known as the *Rao-Blackwellized particle filter*.

5.3 Map representation

Different SLAM algorithms have different map representations and implementations. In very general setting, a map can be represented and stored as M data points each fitting in constant memory. The way the map is stored affects the memory requirements and map access operations. Dense square grid maps in $\mathbb{R}^d$ are represented by $M = N^d$ grid cells, where N is the number of grid cells along a dimension. In $\mathbb{R}^2$, this yields a memory requirement of $O(N^2)$ for a single map. Such representation is justifiable and used in many application domains, as an array implementation yields very fast map access operations and very large arrays fit in the memory of a modern computer. For example, many laser-based approaches [95, 155, 156] store the map as an occupation grid [161]. Grid-based map representations, often accompanied with interpolation, are also adopted in MF localization [13, 25, 42, 45, 57, 60].

In order to save memory, the grid map may be made sparse and stored in a spatial search hierarchy [84]. Quadtrees have been used to represent sparse 2D occupancy grid maps for laser-range data [162, 163]. Similarly, octrees have been used for efficient representation of 3D environments [164, 165]. Publications I and II take a slightly different approach and store the maps as simple hash map-based adaptive grids, where the state space is quantized into a regular grid and grid cells with measurements are represented by a key-value pair in the hash map. Another way is to model the environment with a very coarse regular grid and interpolate the values in between [12, 13, 31]. Furthermore, many variations of the grid map exist, such as hexagonal hierarchical grid adopted in FootSLAM-algorithms [88, 166].

A grid-free way to implement the map is to store only the measurements Z_n and their coordinates as scattered data. For maps in $\mathbb{R}^d$, the memory requirements depend on the dimension of the measurement d_z, yielding memory requirement of $O(n(d+d_z))$. This means that for high-dimensional measurements, such as laser-scans, the grid approach is often preferable, as the grid cells may often be used to combine information from several measurements [161]. However, for low-dimensional measurements, such as scalars or magnetometer readings, the constant factor d_z is negligible. For maps in $\mathbb{R}^2$, the memory requirements become $O(n)$.

5.3.1 Bottleneck: memory and resampling

Because in RBPF each of the P particles carries its own map, the memory requirements $O(PM)$ of naive implementation may become a bottleneck. In addition, naively implemented resampling means that every time resampling occurs, P maps are copied. This leads to $O(PM)$ time complexity. This can be a huge bottleneck for large maps, such as fine-grained occupancy grids. As magnetic measurements are low-dimensional compared, e.g., to laser scans, the maps built from n measurements typically consume less memory at least when mapping new areas. Despite that, the memory and resampling bottleneck is still present also in RBPF MF-SLAM. In Publications I and II, the non-optimized implementation constrained the number of particles available for SLAM to about 200, which was unable to handle feature-poor SLAM data, although achieving a success rate of $19/20$ in feature-rich environments with careful parameter tuning and heuristics. Being able to use more particles would alleviate this.

One way to tackle the complexity problems above is to keep P and M low. For fine-grained occupancy grids with high M, this means reducing P. Because the choice of proposal distribution affects PF performance considerably, informed proposals have been used for great success [95–97]. Grisetti et al. [96] achieve this by adapting the proposal by utilizing the most recent laser-range measurement. Stachniss et al. [83] analyse the Gaussians used in the informed proposals. The adapted proposals allow very low particle counts, such as $P = 15$ [96], to be used for SLAM.

Another route is to minimize M averaged over particles. In a series of self-improving publications Eliazar and Parr [115, 156, 167] introduce DP-SLAM, a way to effectively store the RBPF occupancy grid maps in a structure called the *ancestry tree* that shares the mutual history of particles. They show in the final paper [156] that the structure may be implemented to have the same asymptotic time complexity $O(AP)$ as localization with a single map, where P is the particle count and A is the number of grid cells accessed per measurement. In addition, empirical data suggests that in practice the memory requirements seem to drop from $O(PM)$ of naive RBPF to $O(M+APC)$ due to the nature of the ancestry tree, where C is a smallish constant ($C < 90$). This allows to use a very large number of particles (e.g., $P = 10,000$). Publication V adopts the ancestry tree idea for MF point cloud maps stored in quadtrees. The approach solves the memory and resampling bottlenecks present in Publications I and II and memory-wise allows using at least three magnitudes more particles. This makes even the feature-poor SLAM data sets solvable.

5.4 Loop closing

As with localization, the accumulating odometric error poses a problem also in SLAM. The unbounded odometric error is visualized in Figure 13 (a). In localization, the accumulated error corrupts only the pose estimate, which can be later corrected, e.g., by re-initialization. By contrast, in SLAM, the error may make the whole map useless, as standard RBPF has no mechanism to correct erroneous maps even if current correct pose is recovered. In order to constrain the accumulating errors, the robot has to eventually return to a previously visited place in the map. This is known as *loop closing* and it is an essential part of SLAM [9, 94, 168]. In laser-based SLAM, "returning" to a previously mapped place does not require the robot to be exactly in the same coordinates, as range sensor readings are able to provide constraints about relative transformations between poses [152]. However, for magnetometer-based SLAM, the situation is different. Because the magnetometer measures the field only in one spatial point at a time, the robot has to be very close to the previously measured locations before it can be considered being in a mapped area. The distance depends on the map uncertainty, which in its turn depends on the magnetic landscape and the number of samples in the map. The uncertainty can be very high especially at the beginning of mapping. In order to close loops, it is essential for MF-SLAM that the trajectory intersects itself several times until a good enough map function is obtained.

In many MF-SLAM and localization papers, either implicitly or explicitly, an assumption is made that the trajectories will have significant segments that will be both parallel and overlapping [13, 16, 28, 49, 88, 142, 143, 158, 169]. This makes the corresponding map matching problem one-dimensional in nature. As such, it also becomes considerably easier. This is a fair assumption in many cases, especially when other sensors are used to constraint the movement or the movement is geometrically constrained. For example, laser-based sensing may be used to keep the robot in the middle of corridors. The assumption also makes it possible to use some methodologies, e.g., dynamic time warping [28, 142, 143], that are not directly applicable for the non-constrained case. However, in general case of mapping, a 2D area with magnetometer as the only sensor, parallel and overlapping paths are hard to guarantee. This work makes no such assumptions about the geometry or trajectories.

The FootSLAM line of work by Robertson et al. [88, 166], that successfully uses foot-mounted sensor for RBPF SLAM purposes, relies explicitly and extensively on the assumption that natural human trajectories avoid walls and form a hexagonal transition map based on the assumption. Jung et al. [158, 169] perform graph-based magnetic loop closing by driving the robot on simple rectangular or eight-shaped paths in such a way that significant parts of the trajectory are parallel and overlapping. From these paths, batches of measurements are obtained for comparison in graph-optimization.

Active loop closing tries to return the robot to already mapped areas before the uncertainty grows too large. This has been studied, e.g., by Stachniss et al. [168] for occupancy grid maps. In MF-SLAM context, active loop closing would be very beneficial, as it would often generate overlapping and even parallel paths that are easy to match. Exploration-based strategies evaluated in simulation proposed by Kemppainen et al. [37] and Ruiz et al. [170] could provide a good starting point for a loop closing solution. However, to the author's knowledge, at the time, no such solution has been validated for MF-SLAM in practice.

5.4.1 Example on MF-based loop closing

The example illustrates the nature and difficulty of loop closing in 2D MF-SLAM and how it depends on both odometric information and measurements. It clarifies further that the full vector measurement model discussed in sections 2.5 and 3.4.4 is very sensitive to yaw differences. To get a clear picture of this, the 200 first time steps of CSE lobby SLAM data are briefly analyzed. A description of the full data and SLAM experiments using it can be found in Publications II and V. Figure 13 (a-b) visualizes the odometry and the partial path chosen for the example, (c) the obtained odometry, and (d) the walk of $\mathbf{z}^{\perp}$. The correct loop closure points depicted in Figure 14 (f) are approximately at time steps $\mathbf{t}_1^{LC} = (10, 120)$ and $\mathbf{t}_2^{LC} = (25, 190)$.

Pairwise Euclidean distances $d_{i,j}^{\mathbf{z}}$ between the measurements are visualized for $||\mathbf{z}_{x,y}||$, $\mathbf{z}_z$, yaw-independent vector $\mathbf{z}^{\perp}$, and full vector $\mathbf{z}_{x,y,z}$ (rotated based on the odometry-given yaw). These are depicted in Figure 14 (a-b, d-e). For visual clarity, the MF differences are again clamped between 0 and 20 μT. Differences in $\mathbf{z}^{\perp}$ and $\mathbf{z}_z$ (a-b) show extreme multimodality. Even from $\mathbf{z}^{\perp}$ and $\mathbf{z}_{x,y,z}$, it is very hard to visually detect the two loop closure points, as there is multiple minima ($\mathbf{z}^{\perp}$) or one minimum missing ($\mathbf{z}_{x,y,z}$) outside the diagonal component. Spatial dissimilarity on such a short path between the odometry-given poses can be approximated by the pairwise Euclidean spatial distances $d_{i,j}$. To account for the uncertain odometry, the distances are further restricted from below to obtain $\hat{d}_{i,j} = \max(d_{i,j}, 0.5)$. That is, states are considered being spatially identical if their distance is below 0.5 m. This roughly models the possible error in odometry in a short path like this and detects approximate possible loop closing points rather well. Naturally, with longer paths, the odometric error constantly grows, as can be seen from the full trajectory in Figure 13 (a). The spatial distance defined by $\hat{d}_{i,j}$ is depicted in Figure 14 (c). When the differences are weighted and heuristically combined with $\sqrt{(d_{i,j}^{\mathbf{z}})^2 + (5.0\hat{d}_{i,j})^2}$, we obtain distance matrices depicted in Figure 14 (f-g). (Actually, this combination corresponds to log-likelihood of two independent likelihood functions.) The correct loop closure points can be now seen more clearly in the yaw-independent combination (f), although there is still multiple modes present. The other point in $\mathbf{t}_1^{LC} = (10, 120)$ still stays hidden in the full vector combination (g).

In conclusion, loop closing in non-constrained 2D environment is not an easy task, as the magnetic landscape is heavily multimodal. However, combining measurements over time with constraining odometry information, loop closing is possible as first demonstrated in Publications I and II. A successful SLAM run with the quadtree map

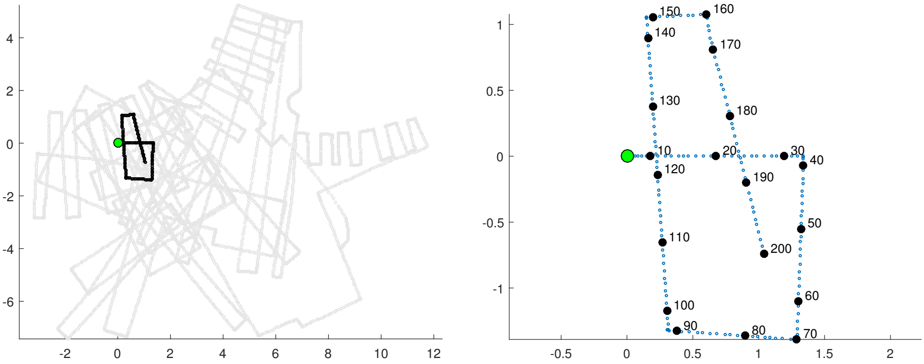

(a) First 200 steps superimposed on the full odometry

(b) First 200 steps of the odometry

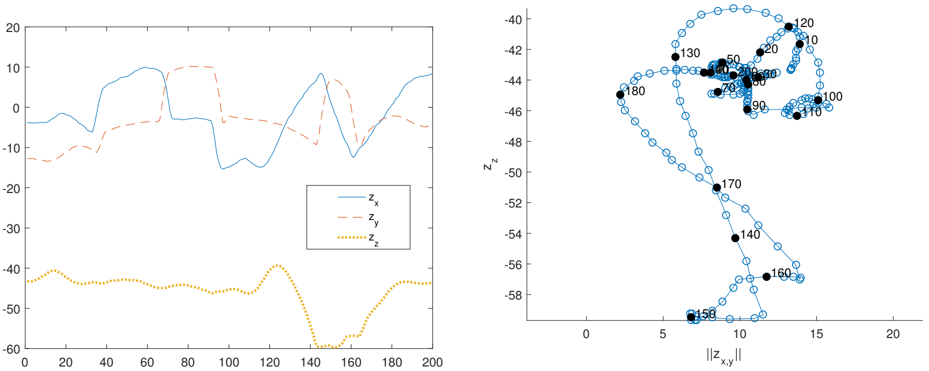

(c) First 200 measurements

(d) Walk of $\mathbf{z}^{\perp} = (||\mathbf{z}_{x,y}||, \mathbf{z}_z)$ over the first 200 measurements

Fig. 13. The first 200 steps of CSE Lobby SLAM data, visualizing the loop closing points (a-b) and the MF data (c-d).

representation from Publication V is demonstrated in Figure 15. Full vector difference is very sensitive to slight yaw-errors, suggesting that a combination of $\mathbf{z}^{\perp}$ and yaw-based likelihood functions could be considered, as discussed in section 3.4.4.

5.5 SLAM in the magnetic field

This section describes some work the author considers most relevant to MF-SLAM. Although all presented research is not directly based on the magnetic field, the methodology and assumptions are so similar that almost direct application to magnetic signatures is possible.

5.5.1 VF-SLAM and its MF derivations

Gutmann et al. [12] propose a very general way to model continuous vector fields on 2D planar environments in conjunction with a method called Vector Field SLAM (VF-SLAM). The field is represented by an automatically updating regular grid of coarse resolution (1-2 m), and bilinear interpolation is used to estimate the vector field values in between. The assumptions made about the vector field signal are very similar to those of MF: *"…the signals change continuously over space, the variability on rotation is independent of position, and the vector of signals provides enough information to estimate pose."* They show that the grid representation is suitable for many different SLAM approaches, such as ESEIF-SLAM [171] and GraphSLAM [152]. The used vector field is generated by Northstar infrared beacon system. Approximately decimeter accuracy is achieved in SLAM experiments with a custom vacuum cleaner in small environments (4×5 m^2). The method is later evaluated in home-sized environments with area of 125 m^2 [32].

Lee et al. [13] utilize the grid-based representation of VF-SLAM for magnetic vector fields. The work strives for better modeling of the indoor MF by using bicubic instead of bilinear interpolation. The SLAM problem is tackled with a RBPF. The feasibility of the proposed approach is verified in simulation and on an actual robot by driving the robot in small environments (7.5–15 m^2) along a boustrophedon and rectangular paths with significant parallel and overlapping segments. Sub-decimeter estimation errors are reported, yielding notable improvement over bilinear interpolation and raw odometry. In another paper [31], also based on VF-SLAM and RBPF, the authors study how the ambiguity of MF observations can be alleviated by using a dual-sensor setup. They use

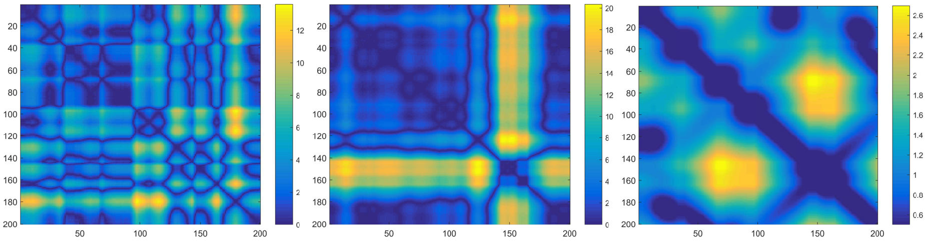

(a) $||\mathbf{z}_{x,y}||$ (b) $\mathbf{z}_z$ (c) $\hat{d}_{i,j}$

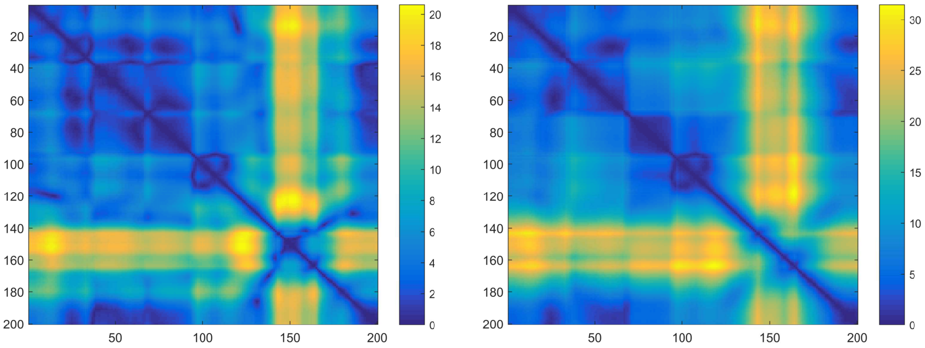

(d) $(||\mathbf{z}_{x,y}||, \mathbf{z}_z)$ (e) $\mathbf{z}_{x,y,z}$

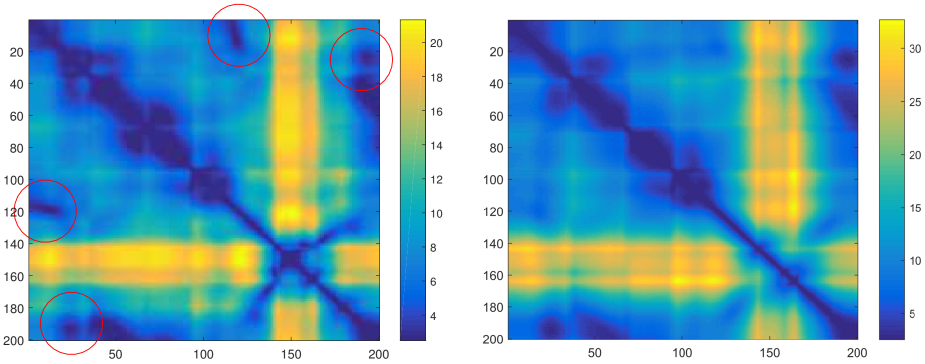

(f) $(||\mathbf{z}_{x,y}||, \mathbf{z}_z)$ and $\hat{d}_{i,j}$ combined and the approximate loop closure points (g) $\mathbf{z}_{x,y,z}$ and $\hat{d}_{i,j}$ combined

Fig. 14. Distance matrices along the 200-step trajectory depicted in Figure 13. The multi-modality illustrates the difficulty of MF-based loop closing even on such a short path.

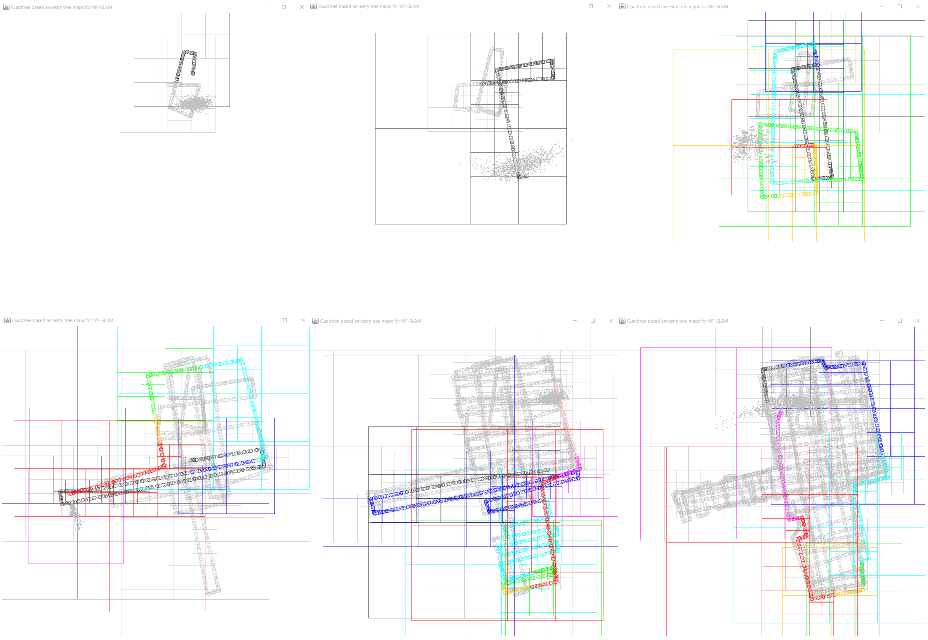

Fig. 15. Snapshots of MF-SLAM in action. Particles are depicted in gray. Only the map of particle $\mathbf{x}^{(1)}$ is visualised. The colors on the path correspond to the ancestry structure in the maps, and the overlapping squares are the quadtrees that store the data points. See Publication V for details.

simulated and real environments similar to the previous study and report significant improvement over single-sensor setup.

5.5.2 Bathymetric SLAM

Although operating on seafloor structures instead of indoor MF landscape, the featureless bathymetric SLAM (BPSLAM) by Barkby et al. [14] is perhaps methodologically most close to Publications I–III and V. The maps are represented by a shared 2D grid similar to DP-SLAM [167] with 1.0 m cell size, and a RBPF is used to solve the SLAM problem to ensure self-consistent seafloor depth maps. Special care is taken not to resample particles, when they have not gathered meaningful information. When a particle arrives to a non-visited grid cell, its measurement there is not considered to match the map either well or poorly. Particles are chosen for resampling based on the ratio of the particle's measurements that are overlapping the previously visited grid cells. The effect of this is similar to the GP variance-based measurement model in

[67] and it is conceptually very close to the conditional weight update in Publications I–II, where the weight was not updated unless the MF estimate was certain enough. The conditional weight update logic in Publications I–II is later made more general in Publication III. The BPSLAM approach is verified on very large data sets, including maps up to approximately 200×350 m^2.

5.5.3 FootSLAM and MagSLAM

FootSLAM by Angermann et al. [166] is a PDR SLAM method based on foot-mounted sensors. It builds heavily on the assumption that natural human motion indoors is constrained by the geometric structure of the building, and that some places, such as corridors and entrances, will be visited more often and are therefore more probable locations for loop closures. This assumption is used to build a probabilistic transition model represented by a hexagonal grid, that together with low level state-of-the-art PDR from the foot-mounted IMU and a RBPF is able to produce geometrically consistent representations of the 2D indoor environment and bound the positioning accuracy to about 2 m level. It is argued that future mobile devices will achieve similar localization accuracy that is achieved with foot-mounted sensors in the study, and that the collaborative and crowd-sourceable version FeetSLAM [172] has the most potential in the future.

Building on FootSLAM, Robertson et al. augment the hexagonal grid cells with magnetic field intensity information to construct a MF-utilizing version of the FootSLAM algorithm, called MagSLAM [88]. The hexagonal grid is further divided into overlapping hierarchical layers of coarse and more fine-grained hexagonal grids in order to model the magnetic field with respect to the local measurement density. Again, a RBPF combined with PDR information is used for solving the SLAM problem. The diameters of the hexagonal bins range from 0.15 m to 0.70 m. The use of magnetic information and hierarchical grids improves the performance significantly: the 2D positioning errors are reported to be in range from 0.1 to 0.2 m.

5.5.4 Graph-based approaches

In a technical report based on his doctoral dissertation, Gao [28] addresses the problem of improving and automating GP-based WiFi and BLE signal map collection for human mapper and consumer-grade smartphones. The work first studies how path-based map collection compares to fingerprint-based manual mapping and concludes that the path-based method can produce comparable maps in a fraction of collection time if the mapping is done densely enough. This is done using paths with known ground truth. The thesis proceeds to propose an offline graph-based SLAM approach, that compares sequences of PDR and MF data to obtain loop closures using DTW. The approach relies explicitly and heavily on the assumption that the map collector follows certain collection guidelines and that majority of the paths are parallel with and overlap previous parts of themselves. The overlapping parts are based on the corridors of the building. In addition, the drift is addressed by straightening the PDR path on a case-by-case basis with a line filter, that assumes straight corridors and a clear angle differences between two corridors. The tested environments are mostly office-like buildings with clear geometric structure, and the approach is able to produce the geometric shape of the floor plan in all of the cases.

Quite surprisingly the author suggests that the use of MF signal should be restricted to the mapping phase, as they have found that MF-based localization is unreliable with consumer-grade smartphones for various reasons, such as decalibration, need for movement, unknown device orientation, and issues in regression. They use the MF signal only to help produce the WiFi and BLE signal maps.

Jung et al. [169] describe a pose graph-based approach that solves the SLAM problem in a small rectangular environment (3×3 m^2) by utilizing sequences of MF data and pose constraints. In addition, to obtain the ground truth, the robot uses a laser range finder to constrain its trajectory implicitly on a rectangular path that provides loop closures in the form of parallel and overlapping MF sequences. In their other work [120] the authors extend the approach to work with similarly constrained longer looping paths (up to 45×56 m^2) and somewhat more complex eight-shaped trajectories in small environments (4×3 m^2).

The path constraints in these graph-based approaches are the main difference compared to the data used in this thesis. To the author's knowledge, there is no research that addresses the MF-SLAM problem with a graph-based SLAM formulation without significant implicit or explicit constraints on the trajectory.

5.6 Conclusions

This chapter has presented the RBPF and efficient map representation methods as the final building blocks needed to implement a fully-working MF-SLAM algorithm for mobile robots in 2D planar indoor environments. Loop closing and the implicit and explicit assumptions taken in different SLAM and localization implementations were discussed, and an illustrating example of MF multimodality in loop closing situation was given. Finally, few selected related works were shortly presented as well.

6 Conclusions and future directions

This overview has shortly presented the problem of magnetic field-based localization and SLAM and the theoretical background of solving the SLAM problem with the Rao-Blackwellized particle filter. The characteristics of the indoor magnetic field and its suitability for localization purposes were addressed. In addition, related research was summarized. The author believes that the literature presented in this overview represents the majority of related work, although magnetic field-based localization and SLAM is a rapidly growing research topic.

In contrast to vision or laser-based SLAM that are very mature research topics and can be considered solved at least in controlled environments [9], the research on MF-SLAM – including this thesis – is still in proof-of-concept stage. There are still several open research questions. How much MF-SLAM can be improved by fusing in other low-costs sensors? In how large environments it can scale to, and how to increase its robustness? Also utilizing the presented methods on completely different sensor modalities, e.g., seafloor depth and vegetation, is left for future research. The thesis tackled the SLAM problem using the RBPF framework, but it is unknown how well, e.g., graph-based SLAM formulation is suited for the problem in larger environments or with less constrained trajectories.

Publications I–II constructed a local GP model of the MF for each particle in every update. In Publication V, a simpler approach was taken by introducing an easy-to-compute local interpolant that was straightforward to use with the ancestry tree map formulation. Being able to effectively compute or approximate a full GP model for each particle could prove very beneficial for MF-SLAM. However, although effective updating for single GP map exists [64], the author is not aware if this can be extended to be used, e.g., with the ancestry tree approach and RBPF SLAM with thousands of particles.

For a SLAM system to be fully autonomous, active localization is needed. Developing such an autonomic system was not unfortunately possible in the limited scope of this thesis. This could be a fruitful direction of future research. Also the applicability of the presented methods for PDR-based systems or mobile devices could be studied. Furthermore, more theoretical analysis of the sampling method presented in Publication IV offers an academically interesting topic.

References

1. Haverinen J & Kemppainen A (2008) Self-localization by utilizing the ambient magnetic field. In: 5th International Conference on Computational Intelligence, Robotics and Autonomous Systems (CIRAS 2008). Linz, Austria.
2. Vaughan R (2008) Massively multi-robot simulation in stage. Swarm Intelligence 2(2-4): 189–208.
3. Vallivaara I, Haverinen J, Kemppainen A & Röning J (2010) Simultaneous localization and mapping using ambient magnetic field. In: Multisensor Fusion and Integration for Intelligent Systems (MFI), 2010 IEEE Conference on, pp. 14–19.
4. Vallivaara I, Haverinen J, Kemppainen A & Röning J (2011) Magnetic field-based SLAM method for solving the localization problem in mobile robot floor-cleaning task. In: Advanced Robotics (ICAR), 2011 15th International Conference on, pp. 198–203.
5. Vallivaara I, Kemppainen A, Poikselkä K & Röning J (2013) Monty Hall particle filter: A new method to tackle predictive model uncertainties. In: Advanced Robotics (ICAR), 2013 16th International Conference on, pp. 1–8.
6. Vallivaara I, Poikselkä K, Rikula P & Röning J (2016) Systematic alias sampling: An efficient and low-variance way to sample from a discrete distribution. ACM Transactions on Mathematical Software (TOMS) 43(3): 18.
7. Vallivaara I, Poikselkä K, Kemppainen A & Röning J (2017) Quadtree-based ancestry tree maps for 2D scattered data SLAM. Manuscript .
8. Thrun S, Burgard W & Fox D (2005) Probabilistic Robotics. MIT Press.
9. Cadena C, Carlone L, Carrillo H, Latif Y, Scaramuzza D, Neira J, Reid I & Leonard JJ (2016) Past, present, and future of simultaneous localization and mapping: Toward the robust-perception age. IEEE Transactions on Robotics 32(6): 1309–1332.
10. Garcia E & Santos PGD (2004) Mobile-robot navigation with complete coverage of unstructured environment. Robotics and Autonomous Systems 46: 195–204.
11. Gerstmayr-Hillen L, Röben F, Krzykawski M, Kreft S, Venjakob D & Möller R (2013) Dense topological maps and partial pose estimation for visual control of an autonomous cleaning robot. Robotics and Autonomous Systems 61(5): 497–516.
12. Gutmann JS, Eade E, Fong P & Munich ME (2012) Vector field SLAM – localization by learning the spatial variation of continuous signals. Robotics, IEEE Transactions on 28(3): 650–667.
13. Lee SM, Jung J & Myung H (2015) Geomagnetic field-based localization with bicubic interpolation for mobile robots. International Journal of Control, Automation and Systems 13(4): 967–977.
14. Barkby S, Williams SB, Pizarro O & Jakuba MV (2011) A featureless approach to efficient bathymetric slam using distributed particle mapping. Journal of Field Robotics 28(1): 19–39.
15. Ferris B, Fox D & Lawrence ND (2007) WiFi-SLAM using Gaussian process latent variable models. In: IJCAI, volume 7, pp. 2480–2485.
16. Haverinen J & Kemppainen A (2009) Global indoor self-localization based on the ambient magnetic field. Robotics and Autonomous Systems 57(10): 1028–1035.

17. Pokémon Go's success adds $7.5 billion to nintendo's market value. `http://www.theverge.com/2016/7/11/12147600/nintendos-stock-pokemon-go`. Accessed: 2016-08-09.
18. MarketsAndMarkets (2014). Indoor location market by positioning systems, maps and navigation, location based analytics, location based services, monitoring and emergency services. worldwide market forecasts and analysis (2014-2019).
19. Lymberopoulos D, Liu J, Yang X, Choudhury RR, Handziski V & Sen S (2015) A realistic evaluation and comparison of indoor location technologies: Experiences and lessons learned. In: Proceedings of the 14th international conference on information processing in sensor networks, pp. 178–189. ACM.
20. Reimann R, Bestmann A & Ernst M (2012) Locating technology for aal applications with direction finding and distance measurement by narrow bandwidth phase analysis. In: International Competition on Evaluating AAL Systems through Competitive Benchmarking, pp. 52–62. Springer.
21. Beder C & Klepal M (2012) Fingerprinting based localisation revisited: A rigorous approach for comparing rssi measurements coping with missed access points and differing antenna attenuations. In: Indoor Positioning and Indoor Navigation (IPIN), 2012 International Conference on, pp. 1–7. IEEE.
22. Li CL, Laoudias C, Larkou G, Tsai YK, Zeinalipour-Yazti D & Panayiotou CG (2013) Indoor geolocation on multi-sensor smartphones. In: Proceeding of the 11th annual international conference on Mobile systems, applications, and services, pp. 503–504. ACM.
23. Chen Y, Lymberopoulos D, Liu J & Priyantha B (2012) Fm-based indoor localization. In: Proceedings of the 10th international conference on Mobile systems, applications, and services, pp. 169–182. ACM.
24. Torres-Sospedra J, Montoliu R, Mendoza G, Belmonte O, Rambla D & Huerta J (2016) Providing databases for different indoor positioning technologies: Pros and cons of magnetic field and wi-fi based positioning. Mobile Information Systems 2016(3-4).
25. Le Grand E & Thrun S (2012) 3-axis magnetic field mapping and fusion for indoor localization. In: Multisensor Fusion and Integration for Intelligent Systems (MFI), 2012 IEEE Conference on, pp. 358–364.
26. Cui Y, An R & Ariyur KB (2015) Cellphone geolocation via magnetic mapping. Automatica 51: 70–79.
27. Alzantot M & Youssef M (2012) CrowdInside: Automatic construction of indoor floorplans. In: Proceedings of the 20th International Conference on Advances in Geographic Information Systems, pp. 99–108.
28. Gao C (2017) Signal maps for smartphone localisation. Technical report, University of Cambridge, Computer Laboratory.
29. IndoorAtlas, indoor positioning service. `http://www.indooratlas.com/`. Accessed: 2017-01-09.
30. Aquamarine robots, robotic solutions for water measurements. `http://www.aquamarinerobots.com/`. Accessed: 2017-01-09.
31. Lee SM, Jung J, Kim S, Kim IJ & Myung H (2015) DV-SLAM (Dual-Sensor-Based Vector-Field SLAM) and observability analysis. IEEE Transactions on Industrial Electronics 62(2): 1101–1112.
32. Gutmann JSR, Goel D & Munich ME (2013) Scaling vector field slam to large environments. In: Intelligent Autonomous Systems 12, pp. 89–100. Springer.

33. Vallivaara I (2008) A team ant colony optimization algorithm for the multiple travelling salesmen problem with minmax objective. In: Proceedings of the 27th IASTED International Conference on Modelling, Identification and Control, pp. 387–392. ACTA Press.
34. Poikselkä K, Vallivaara I & Röning J (2015) Evolutionary robotics on Lego NXT platform. In: Tools with Artificial Intelligence (ICTAI), 2015 IEEE 27th International Conference on, pp. 1137–1144. IEEE.
35. Röning J, Haverinen J, Kemppainen A, Morsari H & Vallivaara I (2008) Smart system for distributed sensing. In: 2008 11th International Biennial Baltic Electronics Conference, pp. 21–30. IEEE.
36. Kemppainen A, Haverinen J, Vallivaara I & Röning J (2010) Near-optimal SLAM exploration in Gaussian processes. In: Multisensor Fusion and Integration for Intelligent Systems (MFI), 2010 IEEE Conference on, pp. 7–13.
37. Kemppainen A, Vallivaara I & Röning J (2015) Magnetic field slam exploration: Frequency domain gaussian processes and informative route planning. In: Mobile Robots (ECMR), 2015 European Conference on, pp. 1–7. IEEE.
38. Poikselkä K, Leinonen M, Palosaari J, Vallivaara I, Haverinen J, Röning J & Juuti J (2015) End cap profile optimization of a piezoelectric Cymbal actuator for quasi-static operation by using a genetic algorithm. Journal of Intelligent Material Systems and Structures p. 1045389X14566526.
39. Poikselkä KL, Leinonen M, Palosaari J, Vallivaara I, Röning J & Juuti J (2017) Novel genetically optimised high-displacement piezoelectric actuator with efficient use of active material. Smart Materials and Structures .
40. Yamazaki K, Kato K, Ono K, Saegusa H, Tokunaga K, Iida Y, Yamamoto S, Ashiho K, Fujiwara K & Takahashi N (2003) Analysis of magnetic disturbance due to buildings. IEEE Transactions on Magnetics 39: 3226–3228.
41. Li B, Gallagher T, Dempster AG & Rizos C (2012) How feasible is the use of magnetic field alone for indoor positioning? In: Indoor Positioning and Indoor Navigation (IPIN), 2012 International Conference on, pp. 1–9.
42. Angermann M, Frassl M, Doniec M, Julian BJ & Robertson P (2012) Characterization of the indoor magnetic field for applications in localization and mapping. In: Indoor Positioning and Indoor Navigation (IPIN), 2012 International Conference on, pp. 1–9.
43. Vandermeulen D, Vercauteren C & Weyn M (2013) Indoor localization using a magnetic flux density map of a building. In: The Third International Conference on Ambient Computing, Applications, Services and Technologies, pp. 42–49. Citeseer.
44. Chung J, Donahoe M, Schmandt C, Kim IJ, Razavai P & Wiseman M (2011) Indoor location sensing using geo-magnetism. In: Proceedings of the 9th International Conference on Mobile Systems, Applications, and Services, pp. 141–154. Bethesda, Maryland, USA.
45. Frassl M, Angermann M, Lichtenstern M, Robertson P, Julian BJ & Doniec M (2013) Magnetic maps of indoor environments for precise localization of legged and non-legged locomotion. In: Intelligent Robots and Systems (IROS), 2013 IEEE/RSJ International Conference on, pp. 913–920.
46. Gutmann JS, Brisson G, Eade E, Fong P & Munich M (2010) Vector field SLAM. In: Robotics and Automation (ICRA), 2010 IEEE International Conference on, pp. 236–242.
47. Storms W, Shockley J & Raquet J (2010) Magnetic field navigation in an indoor environment. In: Ubiquitous Positioning Indoor Navigation and Location Based Service (UPINLBS), 2010, pp. 1–10.

48. Särkkä S, Tolvanen V, Kannala J & Rahtu E (2015) Adaptive kalman filtering and smoothing for gravitation tracking in mobile systems. In: Indoor Positioning and Indoor Navigation (IPIN), 2015 International Conference on, pp. 1–7. IEEE.
49. Suksakulchai S, Thongchai S, Wilkes D & Kawamura K (2000) Mobile robot localization using an electronic compass for corridor environment. In: Systems, Man, and Cybernetics, 2000 IEEE International Conference on, volume 5, pp. 3354–3359.
50. Martinez DM, Haverinen J & Roning J (2008) Sensor and connectivity board (scb) for mobile robots. In: 2008 11th International Biennial Baltic Electronics Conference, pp. 175–178. IEEE.
51. Bradford H (2002). Essentials of geophysics (MIT lecture notes). URL `http://www-gpsg.mit.edu/12.201_12.501/`.
52. International Geomagnetic Reference Field (IGRF). URL `http://www.ngdc.noaa.gov/IAGA/vmod/home.html`.
53. Subbu P & Sasidhar K (2011) Indoor localization using magnetic fields. University of North Texas.
54. Subbu KP, Gozick B & Dantu R (2011) Indoor localization through dynamic time warping. In: Systems, Man, and Cybernetics (SMC), 2011 IEEE International Conference on, pp. 1639–1644. IEEE.
55. Gozick B, Subbu KP, Dantu R & Maeshiro T (2011) Magnetic maps for indoor navigation. Instrumentation and Measurement, IEEE Transactions on 60(12): 3883–3891.
56. Wahlström N, Kok M, Schön TB & Gustafsson F (2013) Modeling magnetic fields using Gaussian processes. In: Acoustics, Speech and Signal Processing (ICASSP), 2013 IEEE International Conference on, pp. 3522–3526.
57. Navarro D & Benet G (2009) Magnetic map building for mobile robot localization purpose. In: Emerging Technologies Factory Automation, 2009. ETFA 2009. IEEE Conference on, pp. 1–4.
58. Shu Y, Bo C, Shen G, Zhao C, Li L & Zhao F (2015) Magicol: indoor localization using pervasive magnetic field and opportunistic wifi sensing. IEEE Journal on Selected Areas in Communications 33(7): 1443–1457.
59. Berkvens R, Vandermeulen D, Vercauteren C, Peremans H & Weyn M (2014) Feasibility of geomagnetic localization and geomagnetic ratslam. International Journal On Advances in Systems and Measurements 7(1&2): 44–56.
60. Kim SE, Kim Y, Yoon J & Eung Sun Kim ES (2012) Indoor positioning system using geomagnetic anomalies for smartphones. In: Indoor Positioning and Indoor Navigation (IPIN), 2012 International Conference on, pp. 1–5.
61. Hemsley R (2009) Interpolation on a magnetic field. Technical report, Bristol University, Tech. Rep.
62. Rasmussen CE & Williams CKI (2005) Gaussian Processes for Machine Learning (Adaptive Computation and Machine Learning). The MIT Press.
63. Akai N & Ozaki K (2015) Gaussian processes for magnetic map-based localization in large-scale indoor environments. In: IEEE/RSJ Int. Conf. on IROS, in Print.
64. Solin A, Kok M, Wahlström N, Schön TB & Särkkä S (2015) Modeling and interpolation of the ambient magnetic field by gaussian processes. arXiv preprint arXiv:1509.04634 .
65. Kok M, Wahlström N, Schön TB & Gustafsson F (2013) MEMS-based inertial navigation based on a magnetic field map. In: Acoustics, Speech and Signal Processing (ICASSP), 2013 IEEE International Conference on, pp. 6466–6470.

66. Wahlström N (2013) Localization using magnetometers and light sensors. Ph.D. thesis, Linköping University.
67. Canciani A (2016) Absolute positioning using the earth's magnetic anomaly field. Ph.D. thesis, Air Force Institute of Technology, Wright-Patterson AFB, OH, Graduate School of Engineering and Management.
68. Särkkä S (2013) Bayesian filtering and smoothing, volume 3. Cambridge University Press.
69. Gordon NJ, Salmond DJ & Smith AF (1993) Novel approach to nonlinear/non-gaussian bayesian state estimation. In: IEE Proceedings F-Radar and Signal Processing, volume 140, pp. 107–113. IET.
70. Thrun S (2002) Particle filters in robotics. In: Proceedings of the Eighteenth conference on Uncertainty in artificial intelligence, pp. 511–518. Morgan Kaufmann Publishers Inc.
71. Gustafsson F, Gunnarsson F, Bergman N, Forssell U, Jansson J, Karlsson R & Nordlund PJ (2002) Particle filters for positioning, navigation, and tracking. Signal Processing, IEEE Transactions on 50(2): 425–437.
72. Karlsson R & Gustafsson F (2003) Particle filter for underwater terrain navigation. In: IEEE Workshop on Statistical Signal Processing.
73. Karlsson R (2005) Particle filtering for positioning and tracking applications. Linköping University Electronic Press.
74. Bergman N (1999) Recursive bayesian estimation. Department of Electrical Engineering, Linköping University, Linköping Studies in Science and Technology. Doctoral dissertation 579.
75. Gustafsson F (2010) Particle filter theory and practice with positioning applications. IEEE Aerospace and Electronic Systems Magazine 25(7): 53–82.
76. Doucet A & Johansen AM (2009) A tutorial on particle filtering and smoothing: Fifteen years later. Handbook of nonlinear filtering 12(656-704): 3.
77. Arulampalam MS, Maskell S, Gordon N & Clapp T (2002) A tutorial on particle filters for online nonlinear/non-gaussian bayesian tracking. Signal Processing, IEEE Transactions on 50(2): 174–188.
78. Tulsyan A, Gopaluni RB & Khare SR (2016) Particle filtering without tears: A primer for beginners. Computers & Chemical Engineering 95: 130–145.
79. Fox D, Burgard W, Dellaert F & Thrun S (1999) Monte carlo localization: Efficient position estimation for mobile robots. AAAI/IAAI 1999: 343–349.
80. Negenborn R (2003) Robot localization and kalman filters. Ph.D. thesis, Utrecht University.
81. Karlsson R & Gustafsson F (2006) Bayesian surface and underwater navigation. IEEE Transactions on Signal Processing 54(11): 4204–4213.
82. Thrun S, Fox D, Burgard W & Dellaert F (2001) Robust monte carlo localization for mobile robots. Artificial intelligence 128(1): 99–141.
83. Stachniss C, Grisetti G, Burgard W & Roy N (2007) Analyzing gaussian proposal distributions for mapping with rao-blackwellized particle filters. In: Intelligent Robots and Systems, 2007. IROS 2007. IEEE/RSJ International Conference on, pp. 3485–3490. IEEE.
84. Samet H (2006) Foundations of multidimensional and metric data structures. Morgan Kaufmann.
85. Crisan D & Doucet A (2002) A survey of convergence results on particle filtering methods for practitioners. IEEE Transactions on signal processing 50(3): 736–746.
86. Tribelhorn B & Dodds Z (2007) Evaluating the roomba: A low-cost, ubiquitous platform for robotics research and education. In: Robotics and Automation, 2007 IEEE International

Conference on, pp. 1393–1399. Roma.

87. Haverinen J & Kemppainen A (2011) A geomagnetic field based positioning technique for underground mines. In: Robotic and Sensors Environments (ROSE), 2011 IEEE International Symposium on, pp. 7–12. IEEE.
88. Robertson P, Frassl M, Angermann M, Doniec M, Julian BJ, Garcia Puyol M, Khider M, Lichtenstern M & Bruno L (2013) Simultaneous localization and mapping for pedestrians using distortions of the local magnetic field intensity in large indoor environments. In: Indoor Positioning and Indoor Navigation (IPIN), 2013 International Conference on, pp. 1–10.
89. Liu JS & Chen R (1998) Sequential monte carlo methods for dynamic systems. Journal of the American Statistical Association 93: 1032–1044.
90. Doucet A, de Freitas N & Gordan N (2001) Sequential Monte Carlo Methods in Practice. Springer-Verlag.
91. Douc R & Cappé O (2005) Comparison of resampling schemes for particle filtering. In: Image and Signal Processing and Analysis, 2005. ISPA 2005. Proceedings of the 4th International Symposium on, pp. 64–69. IEEE.
92. Hol JD, Schon TB & Gustafsson F (2006) On resampling algorithms for particle filters. In: Nonlinear Statistical Signal Processing Workshop, 2006 IEEE, pp. 79–82. IEEE.
93. Doucet A, Godsill S & Andrieu C (2000) On sequential monte carlo sampling methods for bayesian filtering. Statistics and computing 10(3): 197–208.
94. Grisetti G, Stachniss C & Burgard W (2007) Improved techniques for grid mapping with rao-blackwellized particle filters. IEEE transactions on Robotics 23(1): 34–46.
95. Hahnel D, Burgard W, Fox D & Thrun S (2003) An efficient fastslam algorithm for generating maps of large-scale cyclic environments from raw laser range measurements. In: Intelligent Robots and Systems, 2003.(IROS 2003). Proceedings. 2003 IEEE/RSJ International Conference on, volume 1, pp. 206–211. IEEE.
96. Grisetti G, Stachniss C & Burgard W (2005) Improving grid-based slam with rao-blackwellized particle filters by adaptive proposals and selective resampling. In: Robotics and Automation, 2005. ICRA 2005. Proceedings of the 2005 IEEE International Conference on, pp. 2432–2437. IEEE.
97. Grzonka S, Plagemann C, Grisetti G & Burgard W (2009) Look-ahead proposals for robust grid-based slam with rao-blackwellized particle filters. Int. J. Rob. Res. 28(2): 191–200.
98. Philomin V, Duraiswami R & Davis L (2000) Quasi-random sampling for condensation. In: European Conference on Computer Vision, pp. 134–149. Springer.
99. Niederreiter H (1992) Random number generation and quasi-Monte Carlo methods, volume 63. SIAM.
100. Ormoneit D, Lemieux C & Fleet DJ (2001) Lattice particle filters. In: Proceedings of the Seventeenth conference on Uncertainty in artificial intelligence, pp. 395–402. Morgan Kaufmann Publishers Inc.
101. Gerber M & Chopin N (2015) Sequential quasi monte carlo. Journal of the Royal Statistical Society: Series B (Statistical Methodology) 77(3): 509–579.
102. Walker AJ (1977) An efficient method for generating discrete random variables with general distributions. ACM Transactions on Mathematical Software (TOMS) 3(3): 253–256.
103. Solin A, Särkkä S, Kannala J & Rahtu E (2016) Terrain navigation in the magnetic landscape: Particle filtering for indoor positioning. In: Navigation Conference (ENC), 2016 European, pp. 1–9. IEEE.

104. Lawler GF & Puckette EE (2000) The intersection exponent for simple random walk. Combinatorics, Probability and Computing 9(05): 441–464.
105. Madras N & Slade G (2013) The self-avoiding walk. Springer Science & Business Media.
106. Melzak Z (1970) Self-intersections in continuous random walk. Bulletin of the American Mathematical Society 76(6): 1251–1252.
107. Kutler MB, Rogers M & Pippenger N (2015) Self-intersections of two-dimensional equilateral random walks and polygons. arXiv preprint arXiv:1508.05992 .
108. Lu H, Zhao J, Li X & Li J (2007) A new method of double electric compass for localization. In: Proceedings of the 6th world congress on intelligent control and automation.
109. Kim HD, Seo SW, Jang Ih & Sim KB (2007) SLAM of mobile robot in the indoor environment with digital magnetic compass and ultrasonic sensors. In: Control, Automation and Systems, 2007. ICCAS '07. International Conference on, pp. 87–90.
110. Afzal MH, Renaudin V & Lachapelle G (2011) Magnetic field based heading estimation for pedestrian navigation environments. In: Indoor Positioning and Indoor Navigation (IPIN), 2011 International Conference on, pp. 1–10. IEEE.
111. Grzonka S, Dijoux F, Karwath A & Burgard W (2010) Mapping indoor environments based on human activity. In: Proc. IEEE International Conference on Robotics and Automation (ICRA). Anchorage, Alaska.
112. Gao C & Harle R (2015) Sequence-based magnetic loop closures for automated signal surveying. In: Indoor Positioning and Indoor Navigation (IPIN), 2015 International Conference on, pp. 1–12.
113. Bird J & Arden D (2011) Indoor navigation with foot-mounted strapdown inertial navigation and magnetic sensors [emerging opportunities for localization and tracking]. Wireless Communications, IEEE 18(2): 28–35.
114. Biswas J & Veloso M (2013) Multi-sensor mobile robot localization for diverse environments. In: Robot Soccer World Cup, pp. 468–479. Springer.
115. Eliazar A, Parr R *et al.* (2004) Dp-slam 2.0. In: Robotics and Automation, 2004. Proceedings. ICRA'04. 2004 IEEE International Conference on, volume 2, pp. 1314–1320. IEEE.
116. Hähnel D, Schulz D & Burgard W (2003) Mobile robot mapping in populated environments. Advanced Robotics 17(7): 579–597.
117. Li Y, He Z, Nielsen J & Lachapelle G (2015) Using wi-fi/magnetometers for indoor location and personal navigation. In: Indoor Positioning and Indoor Navigation (IPIN), 2015 International Conference on, pp. 1–7. IEEE.
118. Zhang H & Martin F (2011) Robotic mapping assisted by local magnetic field anomalies. In: Technologies for Practical Robot Applications (TePRA), 2011 IEEE Conference on, pp. 25–30.
119. Jung J, Lee SM & Myung H (2014) Indoor mobile robot localization using ambient magnetic fields and range measurements. In: Robot Intelligence Technology and Applications 2, pp. 137–143. Springer.
120. Jung J, Lee SM & Myung H (2015) Indoor mobile robot localization and mapping based on ambient magnetic fields and aiding radio sources. IEEE Transactions on Instrumentation and Measurement 64(7): 1922–1934.
121. Johnsen S & Lohmann KJ (2008) Magnetoreception in animals. Physics Today 61(3): 29.
122. Winklhofer M (2010) Magnetoreception. Journal of the Royal Society Interface 7(Suppl 2): S131–S134.

123. Wiltschko R (2012) Magnetic orientation in animals, volume 33. Springer Science & Business Media.
124. Mora CV, Davison M, Wild JM & Walker MM (2004) Magnetoreception and its trigeminal mediation in the homing pigeon. Nature 432(7016): 508–511.
125. Wiltschko W & Wiltschko R (2005) Magnetic orientation and magnetoreception in birds and other animals. Journal of Comparative Physiology A 191(8): 675–693.
126. Wang Y, Pan Y, Parsons S, Walker M & Zhang S (2007) Bats respond to polarity of a magnetic field. Proceedings of the Royal Society of London B: Biological Sciences 274(1627): 2901–2905.
127. Quinn TP (1980) Evidence for celestial and magnetic compass orientation in lake migrating sockeye salmon fry. Journal of Comparative Physiology 137(3): 243–248.
128. Cain SD, Boles LC, Wang JH & Lohmann KJ (2005) Magnetic orientation and navigation in marine turtles, lobsters, and molluscs: concepts and conundrums. Integrative and Comparative Biology 45(3): 539–546.
129. Boles LC & Lohmann KJ (2003) True navigation and magnetic maps in spiny lobsters. Nature 421(6918): 60–63.
130. Kisliuk M & Ishay J (1977) Influence of an additional magnetic field on hornet nest architecture. Experientia 33(7): 885–887.
131. Banks AN & Srygley RB (2003) Orientation by magnetic field in leaf-cutter ants, atta colombica (hymenoptera: Formicidae). Ethology 109(10): 835–846. URL `http://dx.doi.org/10.1046/j.0179-1613.2003.00927.x`.
132. Jacklyn P & Munro U (2002) Evidence for the use of magnetic cues in mound construction by the termite amitermes meridionalis (isoptera: Termitinae). Australian Journal of Zoology 50(4): 357–368.
133. Qin S, Yin H, Yang C, Dou Y, Liu Z, Zhang P, Yu H, Huang Y, Feng J, Hao J *et al.* (2015) A magnetic protein biocompass. Nature materials .
134. Tyrén C (1982) Magnetic anomalies as a reference for ground-speed and map-matching navigation. Journal of Navigation 35(02): 242–254.
135. Tyrén C (1987) Magnetic terrain navigation. In: Unmanned Untethered Submersible Technology, Proceedings of the 1987 5th International Symposium on, volume 5, pp. 245–256. IEEE.
136. McKay C & Luong T (1998) Localization of mobile robots using magnetic fields. Undergraduate Thesis, McGill University, Canada .
137. Haverinen J & Kemppainen A (2009) A global self-localization technique utilizing local anomalies of the ambient magnetic field. In: IEEE International Conference on Robotics and Automation, pp. 3142–3147. Kobe, Japan.
138. Rahok SA & Koichi O (2009) Odometry correction with localization based on landmarkless magnetic map for navigation system of indoor mobile robot. In: Autonomous Robots and Agents, 2009. ICARA 2009. 4th International Conference on, pp. 572–577.
139. Karlsson R & Gustafsson F (2003) Particle filter for underwater terrain navigation. In: Statistical Signal Processing, 2003 IEEE Workshop on, pp. 526–529.
140. Anonsen KB & Hallingstad O (2006) Terrain aided underwater navigation using point mass and particle filters. In: Proceedings of the IEEE/ION Position Location and Navigation Symposium, pp. 1027–1035.
141. Saxena A & Zawodniok M (2014) Indoor positioning system using geo-magnetic field. In: 2014 IEEE International Instrumentation and Measurement Technology Conference

(I2MTC) Proceedings, pp. 572–577.

142. Riehle TH, Anderson SM, Lichter PA, Condon JP, Sheikh SI & Hedin DS (2011) Indoor waypoint navigation via magnetic anomalies. In: 2011 Annual International Conference of the IEEE Engineering in Medicine and Biology Society, pp. 5315–5318.
143. Shahidi S & Valaee S (2015) GIPSy: Geomagnetic indoor positioning system for smartphones. In: Indoor Positioning and Indoor Navigation (IPIN), 2015 International Conference on, pp. 1–7.
144. Hellmers H, Norrdine A, Blankenbach J & Eichhorn A (2013) An IMU/magnetometer-based indoor positioning system using Kalman filtering. In: Indoor Positioning and Indoor Navigation (IPIN), 2013 International Conference on, pp. 1–9.
145. Wang H, Sen S, Elgohary A, Farid M, Youssef M & Choudhury RR (2012) No need to war-drive: Unsupervised indoor localization. In: Proceedings of the 10th International Conference on Mobile Systems, Applications, and Services, pp. 197–210.
146. Galván-Tejada CE, García-Vázquez JP & Brena R (2013) Magnetic-field feature extraction for indoor location estimation. In: Ubiquitous Computing and Ambient Intelligence. Context-Awareness and Context-Driven Interaction: 7th International Conference on, pp. 9–16.
147. Lau TK, Cheuk Cm, Liu Yh & Lin Kw (2013) Turtle-inspired localization on robot. In: 2013 IEEE/RSJ International Conference on Intelligent Robots and Systems, pp. 5950–5955. IEEE.
148. Blankenbach J & Norrdine A (2010) Position estimation using artificial generated magnetic fields. In: Indoor Positioning and Indoor Navigation (IPIN), 2010 International Conference on, pp. 1–5.
149. Li Y, Zhang P, Niu X, Zhuang Y, Lan H & El-Sheimy N (2015) Real-time indoor navigation using smartphone sensors. In: Indoor Positioning and Indoor Navigation (IPIN), 2015 International Conference on, pp. 1–10.
150. Xiao Z, Wen H, Markham A & Trigoni N (2014) Lightweight map matching for indoor localisation using conditional random fields. In: Information Processing in Sensor Networks, IPSN-14 Proceedings of the 13th International Symposium on, pp. 131–142.
151. Smith R, Self M & Cheeseman P (1987) A stochastic map for uncertain spatial relationships. In: 4th International Symposium on Robotic Research, pp. 467–474.
152. Grisetti G, KÃijmmerle R, Stachniss C & Burgard W (2010) A tutorial on graph-based SLAM. IEEE Intelligent Transportation Systems Magazine 2(4): 31–43.
153. Thrun S, Burgard W & Fox D (2000) A real-time algorithm for mobile robot mapping with applications to multi-robot and 3d mapping. In: Robotics and Automation, 2000. Proceedings. ICRA'00. IEEE International Conference on, volume 1, pp. 321–328. IEEE.
154. Murphy KP *et al.* (1999) Bayesian map learning in dynamic environments. In: NIPS, pp. 1015–1021.
155. Stachniss C, Grisetti G & Burgard W (2005) Information gain-based exploration using rao-blackwellized particle filters. In: In RSS, pp. 65–72.
156. Eliazar A & Parr R (2005) Hierarchical linear/constant time slam using particle filters for dense maps. In: NIPS, pp. 339–346.
157. Montemerlo MS (2003) Fastslam: a factored solution to the simultaneous localization and mapping problem with unknown data association. Ph.D. thesis, Carnegie Mellon University, Pittsburgh, PA, USA. Chair-Whittaker, William and Chair-Thrun, Sebastian.

158. Jung J, Oh T & Myung H (2015) Magnetic field constraints and sequence-based matching for indoor pose graph SLAM. Robotics and Autonomous Systems 70: 92–105.
159. Park BP & Myung H (2014) Underground localization using dual magnetic field sequence measurement and pose graph SLAM for directional drilling. Measurement Science and Technology 25(12): 125101.
160. Mirowski P, Ho TK, Yi S & MacDonald M (2013) SignalSLAM: Simultaneous localization and mapping with mixed WiFi, Bluetooth, LTE and magnetic signals. In: Indoor Positioning and Indoor Navigation (IPIN), 2013 International Conference on, pp. 1–10.
161. Moravec HP (1988) Sensor fusion in certainty grids for mobile robots. AI magazine 9(2): 61.
162. Kraetzschmar GK, Gassull GP, Uhl K, Pags G & Uhl GK (2004) Probabilistic quadtrees for variable-resolution mapping of large environments. In: Proceedings of the 5th IFAC/EURON symposium on intelligent autonomous vehicles. July.
163. Chen Y, Shuai W & Chen X (2015) A probabilistic, variable-resolution and effective quadtree representation for mapping of large environments. In: Advanced Robotics (ICAR), 2015 International Conference on, pp. 605–610. IEEE.
164. Laine S & Karras T (2011) Efficient sparse voxel octrees. IEEE Transactions on Visualization and Computer Graphics 17(8): 1048–1059.
165. Hornung A, Wurm KM, Bennewitz M, Stachniss C & Burgard W (2013) Octomap: An efficient probabilistic 3d mapping framework based on octrees. Autonomous Robots 34(3): 189–206.
166. Angermann M & Robertson P (2012) FootSLAM: Pedestrian simultaneous localization and mapping without exteroceptive sensors – hitchhiking on human perception and cognition. Proceedings of the IEEE 100(Special Centennial Issue): 1840–1848.
167. Eliazar A & Parr R (2003) Dp-slam: Fast, robust simultaneous localization and mapping without predetermined landmarks. In: IJCAI, volume 3, pp. 1135–1142.
168. Stachniss C, Hähnel D, Burgard W & Grisetti G (2005) On actively closing loops in grid-based fastslam. Advanced Robotics 19: 2005.
169. Jung J & Myung H (2015) Pose-sequence-based graph optimization using indoor magnetic field measurements. In: Robot Intelligence Technology and Applications 3, pp. 731–739. Springer.
170. Ruiz AV, Angermann M, Wieser I, Frassl M & Mueller J (2014) Efficient multi-agent exploration with gaussian processes. In: Australasian Conference on Robotics and Automation (ACRA).
171. Walter MR, Eustice RM & Leonard JJ (2007) Exactly sparse extended information filters for feature-based slam. The International Journal of Robotics Research 26(4): 335–359.
172. Robertson P, Puyol MG & Angermann M (2011) Collaborative pedestrian mapping of buildings using inertial sensors and footslam. In: ION GNSS, pp. 1366–1377.

Original articles

I Vallivaara I, Haverinen J, Kemppainen A & Röning J (2010) Simultaneous localization and mapping using ambient magnetic field. In: Multisensor Fusion and Integration for Intelligent Systems (MFI), 2010 IEEE Conference on, pp. 14–19

II Vallivaara I, Haverinen J, Kemppainen A & Röning J (2011) Magnetic field-based SLAM method for solving the localization problem in mobile robot floor-cleaning task. In: Advanced Robotics (ICAR), 2011 15th International Conference on, pp. 198–203

III Vallivaara I, Kemppainen A, Poikselkä K & Röning J (2013) Monty Hall particle filter: A new method to tackle predictive model uncertainties. In: Advanced Robotics (ICAR), 2013 16th International Conference on, pp. 1–8

IV Vallivaara I, Poikselkä K, Rikula P & Röning J (2016) Systematic alias sampling: An efficient and low-variance way to sample from a discrete distribution. ACM Transactions on Mathematical Software (TOMS) 43(3): 18

V Vallivaara I, Poikselkä K, Kemppainen A & Röning J (2017) Quadtree-based ancestry tree maps for 2D scattered data SLAM. Manuscript

Reprinted with permission from IEEE (I–III) and ACM (IV).

Original publications are not included in the electronic version of the dissertation.

625. Visuri, Ville-Valtteri (2017) Mathematical modelling of chemical kinetics and rate phenomena in the AOD Process
626. Lappi, Tuomas (2017) Formation and governance of a healthy business ecosystem
627. Samarakoon, Sumudu (2017) Learning-based methods for resource allocation and interference management in energy-efficient small cell networks
628. Pargar, Farzad (2017) Resource optimization techniques in scheduling : applications to production and maintenance systems
629. Uusitalo, Pauliina (2017) The bound states in the quantum waveguides of shape Y, Z, and C
630. Palosaari, Jaakko (2017) Energy harvesting from walking using piezoelectric cymbal and diaphragm type structures
631. Mononen, Petri (2017) Socio-economic impacts of a public agency – enhancing decision support for performance management
632. Kärkkäinen, Marja-Liisa (2017) Deactivation of oxidation catalysts by sulphur and phosphorus in diesel and gas driven vehicles
633. Viittala, Harri (2017) Selected methods for WBAN communications — FM-UWB and SmartBAN PHY
634. Akram, Saad Ullah (2017) Cell segmentation and tracking via proposal generation and selection
635. Ylimäki, Markus (2017) Methods for image-based 3-D modeling using color and depth cameras
636. Bagheri, Hamidreza (2017) Mobile clouds: a flexible resource sharing platform towards energy, spectrum and cost efficient 5G networks
637. Heikkinen, Kari-Pekka (2018) Exploring studio-based higher education for T-shaped knowledge workers, case LAB studio model
638. Joshi, Satya Krishna (2018) Radio resource allocation techniques for MISO downlink cellular networks
639. Shashika Manosha Kapuruhamy Badalge, (2018) Convex optimization based resource allocation in multi-antenna systems
640. Koskela, Pekka (2018) Energy-efficient solutions for wireless sensor networks
641. Vuokila, Ari (2017) CFD modeling of auxiliary fuel injections in the blast furnace tuyere-raceway area

Book orders:
Granum: Virtual book store
http://granum.uta.fi/granum/

UNIVERSITY OF OULU P.O. Box 8000 FI-90014 UNIVERSITY OF OULU FINLAND

ACTA UNIVERSITATIS OULUENSIS

SERIES EDITORS

A
SCIENTIAE RERUM NATURALIUM
University Lecturer Tuomo Glumoff

B
HUMANIORA
University Lecturer Santeri Palviainen

C
TECHNICA
Postdoctoral research fellow Sanna Taskila

D
MEDICA
Professor Olli Vuolteenaho

E
SCIENTIAE RERUM SOCIALIUM
University Lecturer Veli-Matti Ulvinen

F
SCRIPTA ACADEMICA
Planning Director Pertti Tikkanen

G
OECONOMICA
Professor Jari Juga

H
ARCHITECTONICA
University Lecturer Anu Soikkeli

EDITOR IN CHIEF
Professor Olli Vuolteenaho

PUBLICATIONS EDITOR
Publications Editor Kirsti Nurkkala

UNIVERSITY of OULU
OULUN YLIOPISTO

ISBN 978-952-62-1773-4 (Paperback)
ISBN 978-952-62-1774-1 (PDF)
ISSN 0355-3213 (Print)
ISSN 1796-2226 (Online)